Engineering Applications of Artificial Intelligence 132 (2024) 107943

Contents lists available at ScienceDirect

Engineering Applications of Artificial Intelligence

journal homepage: www.elsevier.com/locate/engappai

An effective matheuristic approach for solving the electric traveling salesperson problem with time windows and battery degradation

Raci Berk İslim [a,b], Bülent Çatay [a,b,*]

[a] Faculty of Engineering and Natural Sciences, Sabanci University, Istanbul, Turkey
[b] Smart Mobility and Logistics Lab, Sabanci University, Istanbul, Turkey

ARTICLE INFO

Keywords:
Electric vehicle
Traveling salesperson problem
Time windows
Charge planning
Battery degradation
Matheuristic

ABSTRACT

Battery is a critical component of an electric vehicle (EV) due to its limited useful economic life and high cost. Good recharging and discharging practices through coordinated and improved route planning decisions in logistics operations may constitute a remedy for maintaining good battery health and avoiding fast degradation, hence, cutting down the costs and reducing adverse environmental effects associated with its disposal. In this study, we investigate the influence of battery degradation cost on the route and charge planning of delivery EVs within the context of the Electric Traveling Salesperson Problem with Time Windows (ETSPTW). First, we introduce the ETSPTW and Battery Degradation (ETSPTW-BD) and present its mathematical model. Since the problem is intractable even for small-size problem instances in the presence of battery degradation, we develop a matheuristic approach that integrates the Variable Neighborhood Search algorithm with an exact solver employed for enhancing the heuristic solutions to solve realistic problems in terms of problem size and constraints. Then, we perform an extensive computational study to validate the performance of the proposed matheuristic and provide managerial insights on the role of battery degradation in routing and charging decisions. Our numerical experiments show substantial cost reduction (up to 11%) can be achieved by incorporating battery degradation into the problem as compared to the solutions obtained by minimizing energy consumption only. However, we also observe that the recharge frequency along the tours may increase, which presents an additional operational challenge for logistics service providers.

1. Introduction

Transportation being the second most CO_2 emitting sector in the world (IEA, 2022) has accelerated actions taken by governments to reduce its adverse environmental and societal effects. For example, the European Union (EU) has recently proposed prohibiting the sale of fossil-fuel cars and vans as of 2035 and declared being stick to the agreement in 2022 (Council of the European Union, 2022). Moreover, ICEVs are banned from or penalized for entering many major European city centres, London, Paris, Milan, Wien, Stuttgart as such (urban-accessregulations.eu). Furthermore, many governments have incentivized EV purchases and issued directives to expand the charging infrastructure and improve the electrical network countrywide to avoid negative externalities caused by internal combustion engine vehicles (ICEVs). The initiatives taken by governments have led companies, government agencies and individuals to consider replacing their ICEVs with EVs. The logistics service providers (LSPs) are in the phase of renewing their fleets by acquiring EVs to use them mainly for last-mile deliveries. For instance, Walmart purchased 4500 EVs in 2022 to deliver online orders and has the option to increase that number up to 10,000 (Walmart, 2022). DHL plans to invest 8 billion US Dollars to have 80,000 EVs by 2030, which will increase the proportion of EVs in their last-mile delivery fleet from 18% to 60%. (DHL, 2022).

We only deal with commercial battery EVs in the scope of this study and refer to them as EVs. EVs offer several advantages over ICEVs. They are more efficient at low speeds, make less noise, require fewer maintenance activities and do not emit greenhouse gases. These advantages indicate that EV usage in urban logistics is more favorable than ICEV usage. On the other hand, EVs have certain drawbacks mainly associated with their limited driving range and long recharging time. These disadvantages cause LSPs to have difficulties in carrying out their operations using an EV fleet.

The energy of an EV is supplied by a rechargeable battery whose performance deteriorates over time with discharges and recharges. It

* Corresponding author. Faculty of Engineering and Natural Sciences, Sabanci University, Istanbul, Turkey.
E-mail address: catay@sabanciuniv.edu (B. Çatay).

https://doi.org/10.1016/j.engappai.2024.107943
Received 16 February 2023; Received in revised form 19 December 2023; Accepted 18 January 2024
Available online 16 February 2024

provides a useful economic life of about 2000 cycles (Pelletier et al., 2016). Despite the advances in battery technology, the cost of batteries still constitutes almost 40% of the purchase price of EVs (König et al., 2021). Although battery prices have been on a downward trend in recent years, first Covid-19 and then the Russia-Ukraine war revealed the vulnerability of the supply chain of critical raw materials for battery production, causing prices to rise again (Jin, 2022). Therefore, maintaining good battery health and avoiding fast degradation is of critical importance for LSPs to reduce their operational costs, and considering battery degradation while generating their route plans may help them extend the lifespan of the batteries in their fleet. However, the number of studies in the literature that studied the effect of battery degradation on the route planning of EVs is quite limited.

In this study, we address the Electric Traveling Salesperson Problem with Time Windows and Battery Degradation (ETSPTW-BD) introduced in İslim and Çatay (2022). In the ETSPTW-BD, the tour of an EV is determined by considering the influence of battery degradation (wear) cost. Since İslim and Çatay (2022) showed that the complexity of the problem increased significantly in the presence of battery degradation, we extend their study by proposing an effective solution procedure to solve realistic-size problems. To the best of our knowledge, this constitutes the first study that attempts to make routing and charge planning decisions simultaneously in the presence of time window restrictions for large-size problem instances by taking into account the cost associated with battery degradation. The contributions of this study can be summarized as follows: (i) we develop a Variable Neighborhood Search (VNS)-based matheuristic approach by introducing problem-specific mechanisms to solve the ETSPTW-BD and validate its performance using well-known data from the literature; (ii) we present the mathematical formulation of a subproblem in the solution method to determine optimal recharging plan for a given visiting sequence of customers by considering battery degradation; (iii) we demonstrate that substantial savings can be achieved by incorporating the effect of battery degradation into routing and charging decisions; and (iv) we perform trade-off analyses based on changing problem characteristics and provide managerial insights.

The remainder of this study is organized as follows: Section 2 reviews the related literature. Section 3 provides the technical background on battery degradation and formulates the battery wear cost (WC) function. Section 4 introduces the ETSPTW-BD and presents its mathematical model. Section 5 describes the proposed VNS-based matheuristic approach. Section 6 presents the numerical study and discusses the results. Finally, Section 7 concludes the paper by providing managerial insights and directions for future research.

2. Literature review

The route planning of EVs has been studied in the literature for over a decade. Erdoğan and Miller-Hooks (2012) addressed the routing of alternative fuel vehicles and introduced the Green Vehicle Routing Problem (GVRP) where range anxiety brings in several restrictions to the classical VRP such as limited availability of alternative fuel stations. Schneider et al. (2014) extended the GVRP by considering the fleet of EVs in the presence of time windows and introduced the Electric Vehicle Routing Problem with Time Windows (EVPRPTW) by allowing EVs recharge their batteries fully only. This problem is more challenging since recharging takes longer than refuelling and its duration is dependent on the amount of energy transferred.

Roberti and Wen (2016) introduced the ETSPTW by considering both full and partial recharges and developed a VNS-based solution method to solve it. Keskin and Çatay (2016) extended the EVRPTW by allowing partial recharges and proposed an Adaptive Large Neighborhood Search algorithm. The following aspects have been tackled in the literature within the context of EV route planning: multiple recharge technologies (Felipe et al., 2014; Keskin and Çatay, 2018); nonlinear charging functions (Montoya et al., 2017; Froger et al., 2019; Kancharla and Ramadurai, 2020); location routing (Hof et al., 2017; Schiffer and Walther, 2017); battery swapping (Yang and Sun, 2015; Hof et al., 2017; Raeesi and Zografos, 2020); stochastic recharging times and availability of charge stations (Sweda et al., 2017; Kullman et al., 2018; Keskin et al., 2019, 2021); two echelons (Breunig et al., 2019), internal and external factors affecting energy consumption such as road gradient, travel speed (Goeke and Schneider, 2015), ambient temperature (Rastani et al., 2019), cargo load (Kancharla and Ramadurai, 2020; Rastani and Çatay, 2021); flexible time windows (Taş, 2021; Sadati et al., 2022); multiple objectives (Amiri et al., 2023; Comert and Yazgan, 2023). The reader is referred to Erdelić and Carić (2019) and Küçükoğlu et al. (2021) for a comprehensive review of the relevant literature.

We summarize the relevant literature in Table 1 by classifying the studies with respect to the problems addressed, solution methods developed, size of the problem solved, and the way the battery degradation is considered in the problem. Column 'TW' indicates whether the problem setting involves the customer time window restrictions. CG, ALNS, GA, DP, DEA, and MF under column 'Solution Method' represent column generation, adaptive large neighborhood search, genetic algorithm, dynamic programming, differential evaluation algorithm, and management framework, respectively. MIP denotes the studies in which a mathematical model is formulated and the problem is solved with a commercial solver.

Feng and Figliozzi (2013) and Goeke and Schneider (2015) considered the degradation of batteries in a mixed fleet of EVs and ICEVs from the perspective of their replacement costs. Sassi et al. (2014) set bounds to the discharge and recharge levels by taking into account that batteries degrade faster at extreme state of charge (SOC) values. Schiffer et al. (2021) proposed an integrated planning scheme to achieve both strategic and operational decisions for EV fleets by considering battery degradation in terms of capacity loss. Both studies incorporated the degradation effect into the battery capacity-related constraints in their mathematical formulations but did not take into account the WC in the objective function.

Barco et al. (2017) proposed a two-phase solution method for solving the EVRP associated with an airport shuttle service. Their method constructs the minimum distance EV routes in the first phase, and in the second phase, it finds the charge schedules for these fixed routes by considering battery degradation. Pelletier et al. (2018) formulated a detailed battery degradation cost structure and integrated it into their mathematical model for the charge scheduling of the EVs. Both studies assume that the routes are given a priori and are concerned with battery degradation only when determining the charge schedules.

Battery degradation was also considered in determining the charge schedules and locating recharging stations within the context of the electrification of public transportation systems. Rohrbeck et al. (2018) took into account the replacement of worn batteries in electric buses while deciding the locations of recharging stations. Wang et al. (2020) determined the schedules of electric buses by considering battery capacity loss. Zhang et al. (2021b) demonstrated that battery lifetime, hence lifecycle costs of the electric buses, can be significantly improved if battery aging is taken into account in charging and discharging cycles. Zhang et al. (2021a) proposed a branch-and-price approach to solve the scheduling of electric buses by taking into account battery degradation and non-linear charging profiles. Battery degradation was also tackled by Zeng et al. (2022), Zhou et al. (2022), Saner et al. (2022) and Shehabeldeen et al. (2023) in the scope of charge scheduling of electric buses. Azadeh et al. (2022) attempted to determine the battery sizes and charging station locations for public buses by considering the impact of different charging profiles on battery degradation. Xu et al. (2021) took into account battery WC for the fleet-sizing problem of a car-sharing service provider.

The literature includes only a few recent studies that take into account the influence of battery degradation on the route plans of the delivery EVs. Zang et al. (2022) developed a column generation algorithm to solve the EVRPTW with nonlinear battery WC and solved only

Table 1
Overview of the related literature in chronological order.

Reference	Problem Type				Problem Size				Solution Method	Battery Degradation Perspective
	Routing	Charge Scheduling	Station Location	Fleet Mgmt	Small	Large	Case Study	TW		
Feng and Figliozzi (2013)				✓			✓		MIP	Constant battery replacement cost
Sassi et al. (2014)	✓						✓		Heuristic	Bounds on recharge and discharge level
Goeke and Schneider (2015)	✓			✓	✓	✓		✓	ALNS	Constant battery replacement cost
Barco et al. (2017)		✓		✓			✓		DEA and GA	WC per unit energy depending on SOC & DOD
Pelletier et al. (2018)		✓					✓		MIP	WC per unit energy depending on SOC & DOD
Rohrbeck et al. (2018)			✓				✓		MIP	Constant battery capacity loss
Wang et al. (2020)				✓			✓		DP	Battery capacity loss depending on temperature, DOD, discharging rate
Zhang et al. (2021b)				✓			✓		MF	Constant battery capacity loss & Bounds on recharge and discharge level
Schiffer et al. (2021)	✓		✓	✓			✓	✓	Matheuristic	Constant battery capacity loss
Xu et al. (2021)		✓		✓			✓		MIP	WC per unit energy depending on SOC & DOD
Zhang et al. (2021a)		✓		✓			✓		CG	WC per unit energy depending on SOC & DOD
Zeng et al. (2022)		✓					✓		MIP	WC per unit energy depending on SOC & DOD
Zhou et al. (2022)		✓		✓			✓		MIP	WC per unit energy depending on SOC & DOD
Azadeh et al. (2022)			✓	✓			✓		MIP	Battery capacity loss depending on SOC
Zang et al. (2022)	✓			✓	✓			✓	CG	WC per unit energy depending on SOC & DOD
Guo et al. (2022)	✓		✓		✓	✓	✓		Metaheuristic	WC per unit energy depending on SOC & DOD
İslim and Çatay (2022)	✓				✓			✓	MIP	WC per unit energy depending on SOC & DOD
Saner et al. (2022)		✓					✓		MIP	WC per unit energy depending on SOC & DOD
Shehabeldeen et al. (2023)		✓		✓			✓		MIP	Constant battery capacity loss
This study	✓				✓	✓		✓	**Matheuristic**	**WC per unit energy depending on SOC & DOD**

small-size problems. Since their method was not designed to minimize the fleet size, their results indicated a significant increase in the number of EVs employed in the presence of battery WC. Guo et al. (2022) considered battery degradation in the context of the Location Routing Problem (LRP) where the locations of recharging stations are determined. The authors observed that locating more stations could reduce the battery WC. They did not consider customer time windows, which are common in real-world delivery operations and may greatly influence the route plans and costs. İslim and Çatay (2022) incorporated the effect of battery degradation into the mathematical model of the ETSPTW and provided solutions for small-size benchmark data by using a commercial solver. Their tests revealed the need for effective heuristic methods as the solver could not even solve small-size instances optimally.

In sum, the studies in the literature remain limited to observe the changes in the routes and operational costs in the presence of WC. They either do not involve a sophisticated battery degradation model or do not present an effective solution method to solve realistic problems in terms of problem size and constraints. This research aims at filling that gap by developing an effective matheuristic approach to solve large-size problem instances in the presence of time window restrictions.

3. Battery degradation

In this study, we consider lithium-ion battery packs, which we will refer to as battery hereafter. Cycle and calendar aging are two main concepts associated with battery degradation. The former represents the deterioration of the battery during its discharge and recharge cycles, whereas the latter corresponds to the deterioration when the battery is not in use, i.e. while being stored. Cycle aging is subject to many factors such as temperature, depth of discharge (DOD) and recharging/discharging rates (Pelletier et al., 2017). DOD refers to the amount of energy recharged/discharged divided by battery capacity. On the other hand, calendar aging mainly depends on the temperature of the environment where the battery is stored, duration of storage, and SOC (Barré et al., 2013). SOC refers to the amount of energy on the battery divided by its capacity.

Barré et al. (2013), Pelletier et al. (2017), Xiong et al. (2018), Vermeer et al. (2022), and Timilsina et al. (2023) examined a wide range of battery degradation models in the literature, among which the discrete model devised by Han et al. (2014) is distinguished with its ease of implementation within the linear programming formulation of the ETSPTW. Battery manufacturers specify the lifespan of their batteries as the achievable cycle counts (ACC) for different DOD values where the fully charged battery is discharged systematically. The relationship between ACC and DOD for a lithium-ion battery is illustrated in Fig. 1 (Han et al., 2014). This figure shows that the battery life shortens as the amount of energy discharged increases.

The degradation also depends on the initial SOC before discharging starts. The formulation of Han et al. (2014) distributes the battery price into each unit of energy charged or discharged by considering the initial SOC level before charging or discharging, which is referred to as *unit wear cost*. This formulation can be extended to express the WC function for a finite number of equal-length SOC intervals as follows:

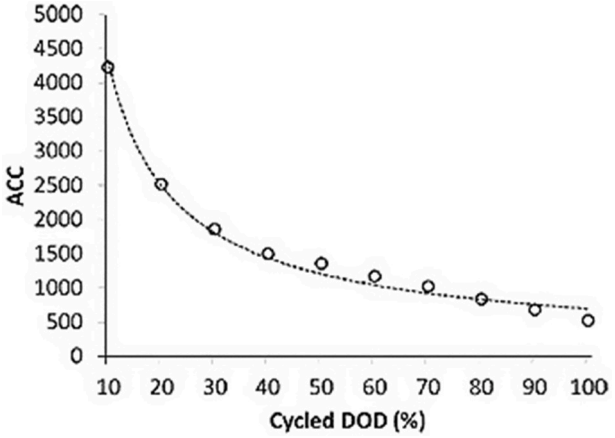

Fig. 1. ACC-DOD graph for a lithium-ion battery (Han et al., 2014).

$$\text{Battery Price} = 2 \times ACC(DOD) \sum_{\substack{d \in D \\ LB^d \geq 1 - DOD}} W(LB^d)\Delta q \quad DOD \in \{L, 2L, \ldots, 1.0\} \tag{1}$$

where $D = \{1, \ldots, n_d\}$ denotes the set of SOC intervals in which each interval $d \in D$ is associated with lower bound LB^d and upper bound UB^d. $W(LB^d)$ is the WC incurred per kWh of energy charged or discharged within the interval $[LB^d, UB^d]$, and Δq represents the amount of energy associated with each SOC interval in kWh. SOC intervals have equal lengths of $L = LB^d - UB^d$ represented in terms of percentage of battery capacity. For example, if DOD intervals of 25% are used (i.e. $L = 0.25$), then four equations for four discrete intervals are formulated as follows:

$$\begin{aligned} W(0.75) &= \frac{\text{Battery Price}}{2 \times ACC(0.25) \times \Delta q} \\ W(0.50) + W(0.75) &= \frac{\text{Battery Price}}{2 \times ACC(0.50) \times \Delta q} \\ W(0.25) + W(0.50) + W(0.75) &= \frac{\text{Battery Price}}{2 \times ACC(0.75) \times \Delta q} \\ W(0.00) + W(0.25) + W(0.50) + W(0.75) &= \frac{\text{Battery Price}}{2 \times ACC(1.00) \times \Delta q} \end{aligned} \tag{2}$$

where Δq corresponds to 25% of the battery energy capacity. By applying the function illustrated in Fig. 1, the ACC values are determined as 2089, 1204, 872 and 694 for DOD values of 25%, 50%, 75%, and 100%, respectively. Then, the WC for each SOC interval $W(LB^d)$ can be calculated given the battery price. In our experimental study presented in Section 6, we use Equation (2) to calculate WC per unit energy charged or discharged within an SOC interval.

Since the $ACC(DOD)$ function decreases with DOD (see Fig. 1), the WC function is non-decreasing according to Equation (1). This means that operating the battery in higher SOCs is more harmful to its state of health (SOH). For instance, consider two equivalent EVs, EV1 and EV2, with initial SOC levels of 40% and 20%, respectively. Suppose that a trip requires 20% DOD and both EVs can feasibly complete it without requiring any recharge. Fig. 2 illustrates the changes in SOC (solid lines) and WC (dotted lines) values observed during the trip of the two vehicles (using the data presented in Section 6.1). We see that although both EVs consume the same amount of energy, EV2 incurs 8.8% less WC compared to EV1 due to the WC function increasing with the initial SOC.

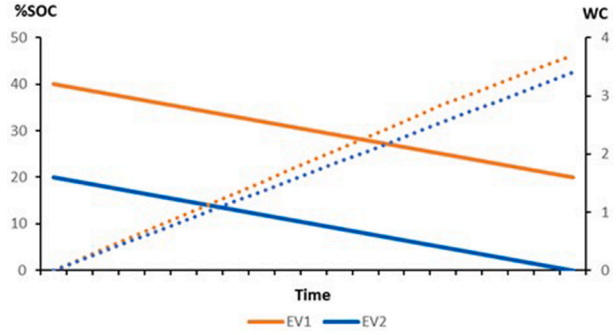

Fig. 2. An illustrative example showing the change in SOCs and wear costs of two EVs with different initial SOCs.

4. Problem description and formulation

The ETSPTW aims at determining the shortest tour of an EV such that all customers are served within their time windows. The EV is allowed to recharge en route at charging stations with any amount of energy such that battery capacity is not exceeded. İslim and Çatay (2022) extended the ETSPTW by taking into account the cost of battery degradation and we refer to the problem as ETSPTW-BD. A single recharging visit is allowed between two consecutive customers, which is a more realistic approach when the industrial practice is considered. Without loss of generality, we assume that the battery of the EV is utilized between 10% and 90% of its capacity and thus the recharging time is linearly proportional to the amount of energy transferred.

Fig. 3 depicts an illustrative example highlighting the advantage of considering battery degradation while making routing decisions. We employ a problem instance (n20w160s5.5) from the dataset described and utilized in the computational study presented in Section 6. This example involves 20 customers and five charging stations. We represent the locations of the depot, customers, and charging stations with a triangle, circles, and charger icons, respectively. To avoid any misunderstanding, a charger icon is put next to the depot since the EV can recharge at the depot as well.

Fig. 3 a shows the optimal tour (tour-1) when the objective function minimizes the total energy consumption. The tour length is 251.41 units and the total cost realized by taking into account the WC is 1043.10. We see that the EV recharges three times along the tour. Fig. 3 b illustrates the tour obtained by incorporating battery WC in the objective function. The total distance traveled is 264.65 units and one more recharging visit takes place along the tour. On the other hand, the total cost is 991.91. So, although the tour length increases, a 4.92% saving in total cost can be achieved by taking into account battery degradation in the problem.

In what follows, we present the mathematical model of the problem introduced by İslim and Çatay (2022) for the sake of completeness. The mathematical notation is based on Roberti and Wen (2016) and Keskin and Çatay (2016). Let $V = \{1, \ldots, n\}$ denote the set of customers and F denote the set of charging stations. The EV starts its journey from node 0 and returns to node $n+1$ where both nodes represent the same depot. We define an augmented set of charging stations F' by copying stations in F to allow multiple visits to each station. The set of nodes and arcs in the problem are as follows: $V_0 = V \cup \{0\}$, $V_{n+1} = V \cup \{n+1\}$, $V_{0,n+1} = V \cup \{0, n+1\}$, $F'_0 = F' \cup \{0\}$, $V' = V \cup F'$, $V'_0 = V' \cup \{0\}$, $V'_{n+1} = V' \cup \{n+1\}$, $V'_{0,n+1} = V'_0 \cup \{n+1\}$ and $A = \{(i,j) | i,j \in V'_{0,n+1}, i \neq j\}$. Thus, we represent the problem on a complete directed graph $G = (V'_{0,n+1}, A)$.

Each customer $i \in V$ is associated with service time s_i and time window $[e_i, l_i]$, where e_i and l_i denote the early and late service starting times at customer i. l_0 is the closing time of the depot and determine the planning horizon. The distance and travel time from node i to node j are denoted by d_{ij} and t_{ij}, respectively. Recharging rate is $1/g$ units of energy per unit time while the consumption is h units of energy per unit distance. The battery capacity is represented by Q and the unit cost of energy is denoted by c.

The decision variables y_i and Y_i keep track of the battery SOC of the EV when it arrives at node $i \in V'_{0,n+1}$ and when it departs from node

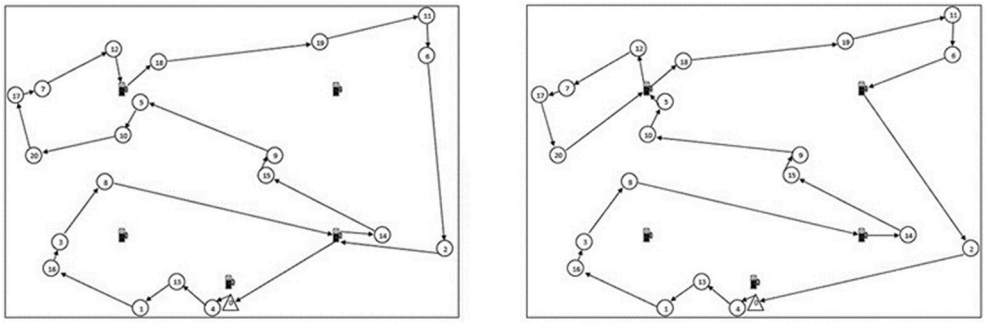

(a) Optimal solution that minimizes energy consumption only (Cost = 1043.10)

(b) Optimal solution that minimizes energy consumption and battery wear cost (Cost = 991.91)

Fig. 3. An illustrative example showing the effect of wear cost in route planning.

$i \in F_0^{'}$, respectively. The binary decision variable x_{ij} is equal to 1 if the arc (i,j) is traversed by the EV and 0 otherwise. The decision variable τ_i represents the service starting time at node $i \in V_{0,n+1}^{'}$. We define two types of decision variables related to battery degradation to express recharges at stations and at the depot overnight. soc_i^d and soc_0^d keep track of how much the portion of SOC interval $d \in D$ used during recharging at a station and at the depot, respectively. The binary decision variables u_i^d and u_0^d are set to 1 if a fraction of SOC interval $d \in D$ is utilized during recharging at a station and at the depot, respectively.

Note that contrary to the common assumption in the literature, we do not set the EV's initial battery level upon its departure from the depot to full capacity since a higher level of battery SOCs results in more battery degradation due to the non-decreasing WC function. Thus, the initial SOC at the departure from the depot is a decision variable. Table 2 summarizes the mathematical notation.

The ETSPTW-BD can be formulated as a 0–1 mixed integer linear programming model as follows:

$$\text{Min } c\left[\sum_{i\in F}(Y_i - y_i) + (Y_0 - y_{n+1})\right] + Q\sum_{d\in D}\left[W^d soc_0^d + \sum_{i\in F} W^d soc_i^d\right] \tag{3}$$

subject to

$$\sum_{\substack{j\in V_{n+1}^{'}\\ i\neq j}} x_{ij} = 1 \quad \forall i \in V_0 \tag{4}$$

$$\sum_{\substack{j\in V_{n+1}\\ i\neq j}} x_{ij} \leq 1 \quad \forall i \in F^{'} \tag{5}$$

$$\sum_{\substack{i\in V_0^{'}\\ i\neq j}} x_{ij} - \sum_{\substack{i\in V_{n+1}^{'}\\ i\neq j}} x_{ji} = 0 \quad \forall j \in V^{'} \tag{6}$$

$$\tau_i + (t_{ij} + s_i)x_{ij} - l_0(1 - x_{ij}) \leq \tau_j \quad \forall i \in V_0, \forall j \in V_{n+1}^{'}, i \neq j \tag{7}$$

$$\tau_i + t_{ij}x_{ij} + g(Y_i - y_i) - (l_0 + g{\cdot}Q)(1 - x_{ij}) \leq \tau_j \quad \forall i \in F^{'}, \forall j \in V_{n+1}, i \neq j \tag{8}$$

$$e_j \leq \tau_j \leq l_j \quad \forall j \in V_{0,n+1}^{'} \tag{9}$$

$$0 \leq y_j \leq y_i - (h{\cdot}d_{ij})x_{ij} + Q(1 - x_{ij}) \quad \forall i \in V, \forall j \in V_{n+1}^{'}, i \neq j \tag{10}$$

$$0 \leq y_j \leq Y_i - (h{\cdot}d_{ij})x_{ij} + Q(1 - x_{ij}) \quad \forall i \in F_0^{'}, \forall j \in V_{n+1}, i \neq j \tag{11}$$

$$y_i \leq Y_i \leq Q \quad \forall i \in F_0^{'} \tag{12}$$

Table 2
Mathematical notation.

Sets	
V	Set of customers
V_0	Set of customers and departure depot
V_{n+1}	Set of customers and arrival depot
$V_{0,n+1}$	Set of customers, departure and arrival depots
F	Set of charging stations
D	Set of SOC intervals
$F^{'}$	Set of charging stations with their copies
$F_0^{'}$	Set of charging stations with their copies and departure depot
$V^{'}$	Set of customers and charging stations with their copies
$V_0^{'}$	Set of customers, departure depot and charging stations with their copies
$V_{n+1}^{'}$	Set of customers, arrival depot and charging stations with their copies
$V_{0,n+1}^{'}$	Set of customers, depots and charging stations with their copies
Parameters	
d_{ij}	Distance between node i and j
t_{ij}	Travel time from node i to node j
s_i	Service time of customer i
$[e_i, l_i]$	Time window of customer i
l_0	Maximum tour duration
Q	Battery capacity
g	Recharging rate
h	Energy consumption per unit distance
c	Unit energy cost
W^d	Wear cost per unit energy charged or discharged within the SOC interval d
L	Length of SOC intervals
UB^d	Upper bound of SOC interval d
LB^d	Lower bound of SOC interval d
Decision variables	
τ_i	Service starting time at node $i \in V_{0,n+1}^{'}$
y_i	Battery SOC of the EV upon arrival at node $i \in V_{0,n+1}^{'}$
Y_i	Battery SOC of the EV during the departure from node $i \in F_0^{'}$
x_{ij}	1 if the EV traverses arc (i,j); 0 otherwise
soc_i^d	Portion of SOC interval $d \in D$ utilized during the recharging at station $i \in F^{'}$
soc_0^d	Portion of SOC interval $d \in D$ utilized during the overnight recharging at the depot
u_i^d	1 if SOC interval $d \in D$ utilized during the recharging at station $i \in F^{'}$; 0 otherwise
u_0^d	1 if SOC interval $d \in D$ utilized during the overnight recharging at the depot; 0 otherwise

$$Q\sum_{d\in D} \text{soc}_i^d = \text{Y}_i\text{-y}_i \quad \forall \text{i} \in \text{F}^{'} \tag{13}$$

$$Q\sum_{d\in D} soc_0^d = Y_0 - y_{n+1} \tag{14}$$

$$0 \leq soc_i^d \leq L{\cdot}u_i^d \quad \forall i \in F^{'}, \forall d \in D \tag{15}$$

$$0 \leq soc_0^d \leq L \cdot u_0^d \quad \forall d \in D \tag{16}$$

$$soc_i^d \leq UB^d - \frac{y_i}{Q} + \left(1 - u_i^d\right) \quad \forall i \in F', \forall d \in D \tag{17}$$

$$soc_0^d \leq UB^d - \frac{y_{n+1}}{Q} + \left(1 - u_0^d\right) \quad \forall d \in D \tag{18}$$

$$x_{ij} \in \{0,1\} \quad \forall i \in V_0', \forall j \in V_{n+1}', i \neq j \tag{19}$$

$$u_i^d \in \{0,1\} \quad \forall i \in F', \forall d \in D \tag{20}$$

$$u_0^d \in \{0,1\} \quad \forall d \in D \tag{21}$$

The objective function (3) minimizes the total cost of energy consumption and battery degradation. The first two terms formulate the cost of energy where the former is associated with energy recharged at stations and the latter corresponds to the energy recharged at the depot before the trip starts. In parallel, the last two terms formulate the WCs associated with recharges at stations and depot, respectively. Constraints (4) make sure that the EV starts its tour from the depot and serves all the customers only once. Constraints (5) ensure that each station is visited at most once. Constraints (6) satisfy the flow conservation at each node. The time feasibility of arcs emanating from the customers/depot and stations are guaranteed by constraints (7) and (8), respectively. Constraints (9) make sure that customer time windows are not violated. Constraints (10) and (11) establish battery SOC consistency when the EV departs from a customer and station/depot, respectively. Constraints (12) guarantee that the battery SOC is not below its initial level and does not exceed the capacity when a station is visited for recharging. The amount of energy recharged at charging stations/depot is distributed to the associated SOC intervals by constraints (13) and (14), respectively. The bounds on the associated SOC intervals to be utilized during the recharges at stations/depot are set by constraints (15) and (16), respectively. Constraints (17) and (18) ensure that an SOC interval takes a positive value if the battery SOC upon arrival at the charging station/depot is less than the upper bound of that SOC interval, respectively. These constraints help avoiding directly assigning values to lower SOC intervals that are cheaper without considering initial SOC values prior to recharging. Finally, constraints (19)–(21) define the binary decision variables.

5. Solution methodology

Since the ETSPTW-BD is intractable in large-size instances, we propose a matheuristic approach, namely MathVNS, which couples the VNS with mathematical programming. MathVNS employs VNS for searching through the promising regions of the TSPTW and determining near-optimal solutions, which are expected to yield high-quality ETSPTW-BD solutions obtained by solving the mathematical model exactly. VNS is a metaheuristic method introduced by Mladenović and Hansen (1997) for solving hard combinatorial optimization problems. The basic VNS consists of two phases: local search (LS) and shaking. LS determines a local optimum in a neighborhood while the neighborhoods around the local optimum found are systematically changed via shaking (Hansen et al., 2010). VNS algorithms have been successfully employed to solve various TSP and VRP variants including the TSPTW (da Silva and Urrutia, 2010; Mladenović et al., 2012), EVRPTW (Schneider et al., 2014), Rich VRPTW (de Armas et al., 2015), ETSPTW (Roberti and Wen, 2016), Hybrid Electric Vehicle TSPTW (Doppstadt et al., 2020), Electric LRP (Hof et al., 2017; Almouhanna et al., 2020), Heterogenous VRPTW under limited resources (Molina et al., 2020), Multi-Depot EVRP (Zhu et al., 2020), Time-Dependent EVRPTW (Lu et al., 2020; Wang et al., 2020), VRP with simultaneous pickup-delivery and time windows (Shi et al., 2020), EVRPTW with time-variant energy prices (Lin et al., 2021), EVRP with Flexible Deliveries (Sadati et al., 2022) and Multi-Mode Hybrid EVRP (Seyfi et al., 2022).

MathVNS starts with the construction of a TSPTW tour using an insertion heuristic. Then, shaking is performed using the first neighborhood structure followed by the LS. If the LS improves the solution, then we fix the sequence of customer visits along the tour and optimize the recharging decisions through a commercial solver by considering the effect of battery degradation. This problem is referred to as the Fixed-Tour Vehicle-Charging Problem with Battery Degradation (FTVCP-BD) and described in Section 5.4. On the other hand, if the LS does not yield a better solution, this procedure is repeated using the following neighborhood structure. To ensure the feasible insertion of recharging station visits along the tour we propose a mechanism that allows slack times at customer visits. Then, the shaking operator is reset to the first neighborhood structure, and this cyclic search procedure is repeated until a pre-determined number of iterations (#*Iter*) is reached or the solution does not improve after performing a pre-determined number of iterations (#*NonImpIter*).

5.1. Initial tour construction

The initial TSPTW tour is constructed using a pseudo-random insertion algorithm. First, we determine the farthest customer from the depot and start the tour. Next, unvisited customers are sorted in non-decreasing order of their late arrival times. Then, a pre-determined number of top-listed customers is considered to select one randomly and add into the tour by using the cheapest insertion approach. If the insertion causes any time-window violation(s), a penalty proportional to the total duration of the violation(s) is added to the corresponding insertion cost. This procedure is repeated until all customers are inserted into the tour.

Since recharges may take significant amounts of time, we propose the *Slack* mechanism to prevent or reduce time window violations resulting from the insertions performed in both initial solution construction and LS. This mechanism brings forward the late service times of the customers in an attempt to promote earlier departures from customers and allow sufficient time for recharges between customer visits. We utilize the length of the planning horizon to determine the length of the slack time proportionally. Suppose that the depot operates from 08:00 to 18:00, hence the planning horizon is 10 h. If *Slack* is set to 1%, it is equivalent to 6 min ($1\,\% \times 10 = 0.1$ hours). Then, the late service times of all customers are reduced by 6 min. For example, if the time window of a customer is [9:00–12:00], it is updated as [9:00–11:54] for planning purposes. The influence of this mechanism is demonstrated in Sections 6.2 and Appendix B.

5.2. Shaking

MathVNS employs λ-*Move* neighborhood structures for shaking, which removes λ randomly selected customers and inserts them to random positions in the tour without seeking time windows feasibility. We also considered λ-*Exchange* that swaps the positions of λ randomly selected customer pairs; however, our preliminary tests showed that it increases the computational effort significantly without providing much improvement in the solution quality. The shaking neighborhoods are illustrated in Fig. 4.

5.3. Local search

MathVNS employs *Move*, *Exchange* and 2-*Opt* neighborhood structures in LS, which are illustrated in Fig. 5. *Move* operator removes a customer and places it into a new position in the tour. *Exchange* operator swaps the positions of two customers in the tour. 2-*Opt* selects two arcs in the tour and reverses the visiting order of customers that are positioned in between.

We also implement restricted candidate lists (RCLs) in the LS, which limit the number of positions that a customer can be inserted in the tour.

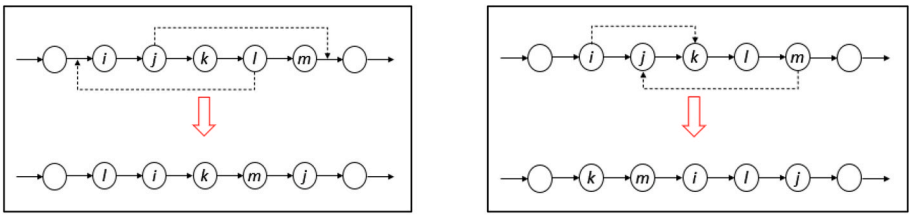

Fig. 4. Illustration of shaking operators.

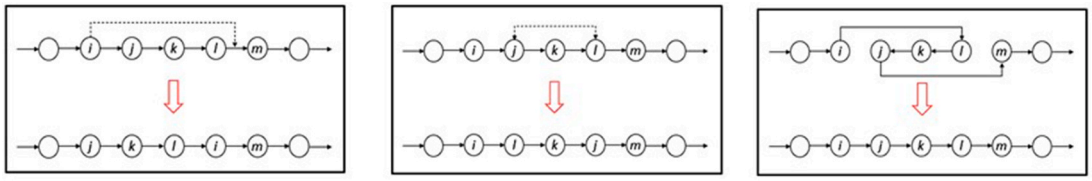

Fig. 5. Illustration of LS operators.

The RCL for a pair of customers comprises a pre-determined number (*RCL Size*) of customers sorted in non-decreasing order of their insertion cost between them. In the LS, thus, a position for a customer node is only evaluated if it is in the RLC of that position. With the implementation of RCLs, the computational effort is reduced by focusing on the promising regions of the solution space.

Algorithm 1. *Local Search*(x,x^*)

```
    Set of LS neighborhood structures l_m (m = 1, ..., m_max)
    m ← 1
1   x' ← x                                  // Incumbent solution
2   while (m ≤ m_max)
3       Apply l_m on x
4       if (cost(x) < cost(x*))
5           Break
6       else if (cost(x) < cost(x'))
7           x' ← x
8           m ← 1
9       Else
10          m++
11      end if
12  end while
13  return x
```

We apply the LS in a cyclic manner, i.e. it returns to the first operator (Move) whenever the solution is improved. As in the construction phase, time-window violations are also penalized in the evaluations. Equipped with the Slack mechanism and penalties associated with time-window violations, the LS is expected to generate good feasible solutions that allow feasible visits to recharging stations without needing a repair algorithm. The pseudocode of the LS is given in Algorithm 1.

5.4. Fixed-Tour Vehicle-Charging Problem with battery degradation (FTVCP-BD)

For a given feasible sequence of customers, i.e. a TSPTW tour, we formulate the FTVCP-BD to optimally plan station visits for recharging and determine the amounts of energy transferred by taking into account the battery degradation. This approach has been successfully employed in the literature within the context of several EVRP variants to determine the recharge visits and the amounts of energy recharged (see Suzuki, 2014; Montoya et al., 2017; Keskin and Çatay, 2018). In this study, we extend it by incorporating the battery wear cost in recharge planning.

The additional notation used in the formulation of the FTVCP-BD is as follows: Let $\overline{V} = \{c_1, c_2, \ldots, c_n\}$ be the ordered set of customers visited by the EV where c_i corresponds to the customer in the i^{th} position of the fixed tour. We define $\overline{V}_0 = \{0\} \cup \overline{V}$ and $\overline{V}_{n+1} = \overline{V} \cup \{n+1\}$. The binary decision variable x_{ij} defined over $i \in \overline{V}_0$ and $j \in F$ is equal to 1 if the EV recharges at station j upon its departure from customer c_i; and 0 otherwise. $\theta_{i,i+1}$ keeps track of the amount of energy transferred if a recharging visit occurs between customers c_i and c_{i+1}.

$$\text{Min } c\left[\sum_{i\in\overline{V}_0}\theta_{i,i+1} + (y_0 - y_{n+1})\right] + Q\sum_{d\in D}\left[W^d soc_0^d + \sum_{i\in\overline{V}_0} W^d soc_{i,i+1}^d\right] \tag{22}$$

subject to

$$\sum_{j\in F} x_{ij} \le 1 \quad \forall i \in \overline{V}_0 \tag{23}$$

$$\tau_i + s_i + t_{i,i+1}\left(1 - \sum_{j\in F} x_{ij}\right) + \sum_{j\in F}(t_{ij} + t_{j,i+1})x_{ij} + g\cdot\theta_{i,i+1} \le \tau_{i+1} \quad \forall i \in \overline{V}_0 \tag{24}$$

$$e_i \le \tau_i \le l_i \quad \forall i \in \overline{V}_{n+1} \tag{25}$$

$$y_i - h\left[d_{i,i+1}\left(1 - \sum_{j\in F} x_{ij}\right) + \sum_{j\in F}(d_{ij} + d_{j,i+1})x_{ij}\right] + \theta_{i,i+1} = y_{i+1} \quad \forall i \in \overline{V}_0 \tag{26}$$

$$y_i - h\sum_{j\in F} d_{ij}x_{ij} \ge 0 \quad \forall i \in \overline{V}_0 \tag{27}$$

$$\theta_{i,i+1} \le Q\sum_{j\in F} x_{ij} \quad \forall i \in \overline{V}_0 \tag{28}$$

$$\theta_{i,i+1} \le Q - \left(y_i - h\sum_{j\in F} d_{ij}x_{ij}\right) \quad \forall i \in \overline{V}_0 \tag{29}$$

$$Q\sum_{d\in D} soc_{i,i+1}^d = \theta_{i,i+1} \quad \forall i \in \overline{V}_0 \tag{30}$$

$$Q\sum_{d\in D} soc_0^d = y_0 - y_{n+1} \tag{31}$$

$$0 \leq soc^d_{i,i+1} \leq L \cdot u^d_{i,i+1} \quad \forall i \in \overline{V}_0, \forall d \in D \tag{32}$$

$$0 \leq soc^d_0 \leq L \cdot u^d_0 \quad \forall d \in D \tag{33}$$

$$soc^d_{i,i+1} \leq UB^d - \frac{1}{Q}\left(y_i - h\sum_{j \in F} d_{ij} x_{ij}\right) + \left(1 - u^d_{i,i+1}\right) \quad \forall i \in \overline{V}_0, \forall d \in D \tag{34}$$

$$soc^d_0 \leq UB^d - \frac{y_{n+1}}{Q} + \left(1 - u^d_0\right) \quad \forall d \in D \tag{35}$$

$$x_{ij} \in \{0,1\} \quad \forall i \in \overline{V}_0, \forall j \in F \tag{36}$$

$$u^d_{i,i+1} \in \{0,1\} \quad \forall i \in \overline{V}_0, \forall d \in D \tag{37}$$

$$u^d_0 \in \{0,1\} \quad \forall d \in D \tag{38}$$

Similar to (3) the objective function (22) minimizes the total cost of the tour. Constraints (23) guarantee that the EV departing from a customer/depot travels to at most one station. Time windows feasibility of customer and depot nodes are satisfied with constraints (24) and (25). Constraints (26) keep track of the battery SOC upon arrival at customer and depot nodes. If a recharging visit takes place between two consecutive customers, constraints (27) ensure that the EV has sufficient energy to reach the charging station upon its departure from the preceding customer. If a charging station is visited between customers c_i and c_{i+1}, then constraints (28) allow positive amount recharging, while constraints (29) limit that amount with available battery capacity. The amounts of energy transferred at charging stations and the depot overnight are distributed to the associated SOC intervals using constraints (30) and (31), respectively. Constraints (32) and (33) set upper and lower bounds on associated SOC intervals for recharges performed at stations and depot, respectively. If the initial battery SOC before the recharging starts at the charging station and depot is less than the upper bound of an SOC interval, then a positive value is assigned to the associated SOC interval by constraints (34) and (35), respectively. Binary decision variables are defined by constraints (36)-(38).

The pseudocode of our solution method is provided in Algorithm 2.

Algorithm 2. MathVNS

```
    y* ← null                                              // Best ETSPTW-BD tour
    y ← null                                               // Current ETSPTW-BD tour
    iterCount ← 0, nonImpIterCount ← 0
    Set of shaking neighborhood structures S_k {k = 1, ..., k_max}
    k ← 1
1   x ← Construct the initial tour
2   x* ← x                                                 // Best TSPTW tour
3   while (iterCount < #Iter) & (nonImpIterCount < #NonImpIter)
4       Generate a random solution x in the k^th neighborhood of x*, S_k(x*)   // Shaking
5       iterCount + +
6       Local Search(x, x*)
7       if (cost(x) < cost(x*))
8           x* ← x
9           k ← 1
10          nonImpIterCount ← 0
11          y ← FTVCP − BD(x*)                             // Determine ETSPTW-BD tour
12      else if (k = k_max)
13          k ← 1
14          nonImpIterCount + +
15      else
16          k + +
17          nonImpIterCount + +
18      end if
19      if (cost(y) < cost(y*))
20          y* ← y                                         // Best ETSPTW-BD tour
21      end if
22  end while
23  return y*
```

6. Experimental study

In this section, we first describe the experimental setting. Then, we present our parameter tuning procedure and validate the performance of the proposed MathVNS. Next, we analyze the effect of battery degradation on routing and recharging decisions and discuss the results. Finally, we investigate the trade-offs associated with problem parameters. We performed our experimental study on a Windows 10 OS computer equipped with an Intel i7-8700 3.20 GHz CPU and 32 GB RAM. The algorithms were coded in Java and the mathematical models were solved using CPLEX 12.9.0 in default mode.

6.1. Data

In our experiments, we employ small- and large-size benchmark datasets from the literature. Our small-size dataset includes 13 single-vehicle EVRPTW instances of Schneider et al. (2014) and ETSPTW instances generated by Roberti and Wen (2016). The former data is classified into three groups involving 5, 10 and 15 customers with varying number of stations and time-window lengths. The latter data consists of 20 customers, and the time window lengths are 120, 140, 160, 180 and 200 time units. There are 5 instances associated with each time-window length and two versions exist each involving 5 and 10 charging stations. Hence, the dataset includes $5 \times 5 \times 2 = 50$ small-size instances in total.

Our large-size dataset is based on the large-size ETSPTW instances that were generated by Roberti and Wen (2016) using the TSPTW instances of Ohlmann and Thomas (2007). This dataset is classified into two groups each involving 5 and 10 charging stations. Each group

Table 3
Examples of tours having the same total distance.

Instance	TD	Tour
n20w120s5.1	271	0,6,16,9,19,17,18,12,10,11,5,1,15,2,21,7,4,13,20,24,3,8,14,21,0
		0,6,16,9,19,17,**22**,18,12,10,11,5,1,15,2,21,7,4,13,20,24,3,8,14,21,0
n20w120s5.2	225	0,1,14,18,4,8,21,19,16,11,15,23,5,7,3,20,17,12,9,10,23,6,2,13,0
		0,1,14,18,4,8,21,19,16,11,15,23,5,7,3,20,17,12,**10**,**9**,23,6,2,13,0
n20w120s5.5	249	0,19,13,11,7,16,18,3,8,21,17,2,5,14,10,4,24,6,9,15,12,22,1,20,0
		0,19,13,11,7,16,18,3,8,21,17,2,5,14,10,4,24,**9**,**6**,15,12,22,1,20,0
		0,19,13,11,7,16,18,3,8,21,17,2,5,**10**,**14**,4,24,6,9,15,12,22,1,20,0
		0,19,13,11,7,16,18,3,8,21,17,2,5,**10**,**14**,4,24,**9**,**6**,15,12,22,1,20,0

comprises 15 instances involving 150 customers and 10 instances involving 200 customers. Hence, the large-size dataset includes $2 \times (15 + 10) = 50$ instances in total. Time window lengths in 150-customer instances vary from 120 to 160 time units and from 120 to 140 time units in 200-customer instances.

Roberti and Wen (2016) provided Euclidean distances rounded to integer values in their dataset; however, they do not necessarily satisfy the triangle property. In the original TSPTW data, the distances were first rounded down to integer values, and then, some adjustments were made to ensure the triangle property. However, these adjustments reduce the distance values, do not guarantee the triangle inequality and may result in overestimation of the costs. Fleming et al. (2013) demonstrated the negative effects of triangular inequality violations on the VRP. Furthermore, Roberti and Wen (2016) introduced charging stations and calculated their distances to customers by rounding them to the nearest integer (instead of rounding them down), thus, caused further inconsistency in the data and violation of triangle property. In addition, we observed that some optimal solutions reported by Roberti and Wen (2016) may not be feasible because of the time window violations when the distances are rounded with higher precision. In addition, different tours may yield the same optimal or best-known objective function value (OFV) in some instances. Hence, differentiating the optimal or best-known tour might not be possible since multiple solutions can have the same OFV. This impairs our solution approach that counts on good TSPTW tours for determining high-quality ETSPTW-BD solutions because the quality of tours having the same (integer) lengths cannot be assessed properly.

Table 3 provides the details of three ETSPTW instances with multiple optima. Under column 'Instance', the numbers next to 'n', 'w' and 's' represent the number of customers, time windows length, and the number of charging stations, respectively, while the number following the dot shows the version of the data. 'TD' indicates the total distance, and the sequence of the nodes visited is reported under column 'Tour', where 0 denotes the depot, nodes 1–20 are the customers, and nodes 21–24 represent the charging stations. The differences in the alternative optimal tours with respect to the first tour presented in the first row for each instance are indicated in bold. For example, inserting charging station 22 between two consecutive customers 17 and 18 (i.e. detouring and visiting an extra node) in instance 'n20w120s5.1' does not increase the (integer) length of the tour. Note that the number of multiple optimal tours increases as the problem size grows. Therefore, we increased the precision and used distances truncated two decimal places. This rounding procedure compared to rounding down to the nearest integer increases the total distance of a tour substantially and may make the problem infeasible because of the strict time windows. Therefore, we extended the length of the planning horizon and late arrival times proportionally. The details can be found in Appendix A. All other data and parameter values remain same as in Roberti and Wen (2016).

We set $n_d = 4$ and $L = 1/4 = 0.25$ following the base case scenario of Pelletier et al. (2018). Hence, the upper and lower bounds of SOC intervals are $LB^d = \{0, 0.25, 0.5, 0.75\}$ and $UB^d = \{0.25, 0.5, 0.75, 1\}$, respectively. Pelletier et al. (2018) considered battery unit cost as \$410/kWh and calculated battery WC for these four intervals as 0.48, 0.52, 0.58 and \$0.79/kWh, respectively. We take the battery unit cost as \$151/kWh (Dempsey, 2022), thus, the WC values for these four intervals are calculated as \$0.17, \$0.19, \$0.21 and \$0.29/kWh, respectively. Moreover, both Schneider et al. (2014) and Roberti and Wen (2016) assumed that the EV travels one unit of distance in one unit of time by consuming one unit of energy. So, we set the unit energy cost $c = 1$ to be able to compare our results with those reported in the literature. Considering the 5-year average industrial electricity price \$0.06892/kWh in the U.S during 2017–2021 (U.S. Energy Information Administration, 2022) we adapted the WCs to our problem by keeping the ratio between the unit energy cost parameter and the unit electricity price as follows: $W^d = \{2.56, 2.78, 3.10, 4.22\}$.

6.2. Parameter tuning

MathVNS employs five parameters, namely λ, *Slack*, *#NonImpIter*, *#Iter*, and *RCL Size*. To tune them, we selected five 150- and five 200-customer ETSPTW-BD instances as follows: n150w120s5.2, n150w140s5.1, n150w140s5.4, n150w160s5.2, n150w160s5.3, n200w120s5.1, n200w120s5.4, n200w120s5.5, n200w140s5.3 and n200w140s5.4. The parameters were sequentially tuned from λ to *RCL Size*. We set the initial values of λ, *Slack*, *#NonImpIter*, *#Iter* and *RCL Size* to 6, 0%, $3n$, $3n$ and n, respectively. To tune each parameter, we performed 25 runs per problem instance and calculated the average percentage deviation from the average of the best solutions obtained (Δ%). The value with the smallest Δ% was selected. If more than one value provides the same Δ%, we favored the smaller value. This procedure was repeated until all parameters had been tuned. The values tested and their corresponding Δ% are presented in Table 4. The selected values are shown in bold.

When solving the small-size instances, we removed the stopping criterion based on the number of non-improving iterations (*#NonImpIter*) and the RCL mechanism since the runtime was not a concern.

6.3. Convergence analysis

We perform an analysis of convergence using five small-size and ten large-size instances. The convergence behaviors are shown in Fig. 6. Fig. 6 an involves small-size instances with 20 customers, whereas Fig. 6 b includes large-size instances with 150- and 200-customers, which are employed in the parameter tuning procedure. The analysis was

Table 4
Parameter tuning.

Parameter	Values (Δ%)					
λ	6	8	10	12	**14**	16
	(0.10)	(0.29)	(0.13)	(0.44)	**(0.00)**	(0.16)
Slack	0%	0.5%	**1%**	1.5%	2%	–
	(1.05)	(0.48)	**(0.00)**	(0.33)	(0.50)	
#NonImpIter	$0.25n$	$0.375n$	$\mathbf{0.5}n$	$0.75n$	n	–
	(0.51)	(0.13)	**(0.00)**	(0.00)	(0.00)	
#Iter	n	$2n$	$3n$	$\mathbf{4}n$	$5n$	–
	(0.43)	(0.36)	(0.13)	**(0.00)**	(0.00)	
RCL Size	$0.05n$	$0.1n$	$\mathbf{0.15}n$	$0.25n$	$0.5n$	n
	(0.16)	(0.08)	**(0.00)**	(0.08)	(0.18)	(0.37)

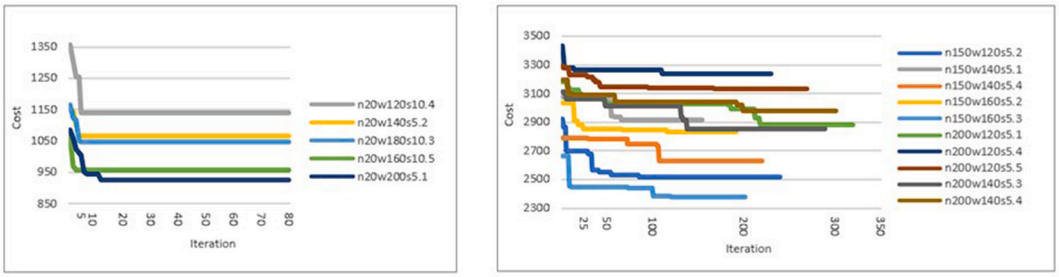

(a) Convergence in small-size instances

(b) Convergence in large-size instances

Fig. 6. Convergence analysis.

performed based on the runs in which the best solutions were obtained with tuned parameters.

6.4. Performance validation

We validated the performance of MathVNS using three problem variants. We performed 25 runs for each instance and considered the best solution in our comparisons.

6.4.1. Validation using TSPTW data

We first investigated the performance of MathVNS on the large-size TSPTW instances of Ohlmann and Thomas (2007). Since the problem does not include EVs, we set *Slack* value to 0% and did not solve the FTVCP-BD throughout the execution of MathVNS. Our algorithm found the best-known solution (BKS) in all 50 instances. Our average runtimes are 22.50 and 61.65 s for 150- and 200- customer-instances, respectively. Since the BKSs were already presented in Da Silva and Urrutia (2010), we do not report them again here.

6.4.2. Validation using ETSPTW data

We also demonstrate the effectiveness of MathVNS in the ETSPTW setting. We compare the solution quality and the runtime of MathVNS with CPLEX in small-size problem instances with 20 customers. We modified our models to minimize the total distance and exclude battery degradation-related constraints and solved it using CPLEX. Since small-size instances have short time horizons, *Slack* has little or no influence on time-window lengths. Therefore, we set it equal to 0% in these experiments. The results are given in Table 5. Column 'TD' shows the optimal tour lengths, column 'CPLEX' presents the runtime of CPLEX in seconds, and column 'MathVNS' reports the average time of 25 runs in seconds. We observe that MathVNS finds the optimal solutions in all instances with significantly less computational effort compared to CPLEX.

6.4.3. Validation using ETSPTW-BD data

The performance of MathVNS is validated by using small-size ETSPTW-BD data as well. The solutions achieved by CPLEX and

Table 5
Comparison of ETSPTW results for 20-customer problems.

		Runtime				Runtime	
Instance	TD	CPLEX	MathVNS	Instance	TD	CPLEX	MathVNS
n20w120s5.1	274.48	3.64	0.56	n20w120s10.1	273.37	2.60	0.54
n20w120s5.2	228.02	386.25	0.63	n20w120s10.2	223.84	302.68	0.37
n20w120s5.3	297.10	6.51	0.29	n20w120s10.3	295.47	9.14	0.24
n20w120s5.4	307.17	91.49	0.28	n20w120s10.4	299.80	17.42	0.27
n20w120s5.5	254.63	2.33	0.32	n20w120s10.5	248.52	2.03	0.31
n20w140s5.1	188.20	17.67	0.16	n20w140s10.1	185.56	9.00	0.16
n20w140s5.2	274.47	153.86	0.25	n20w140s10.2	258.74	104.07	0.23
n20w140s5.3	244.16	30.73	0.16	n20w140s10.3	244.13	23.26	0.18
n20w140s5.4	254.85	536.39	0.64	n20w140s10.4	244.28	39.73	0.53
n20w140s5.5	223.60	2.50	0.34	n20w140s10.5	221.04	4.09	0.33
n20w160s5.1	245.12	9.65	0.32	n20w160s10.1	245.12	19.72	0.28
n20w160s5.2	224.22	17.65	0.23	n20w160s10.2	214.56	13.22	0.21
n20w160s5.3	213.11	1.30	0.29	n20w160s10.3	213.11	2.27	0.28
n20w160s5.4	213.43	30.20	0.32	n20w160s10.4	213.43	44.95	0.31
n20w160s5.5	251.41	40.96	0.60	n20w160s10.5	243.11	27.12	0.50
n20w180s5.1	266.88	63.10	0.46	n20w180s10.1	260.07	35.09	0.38
n20w180s5.2	281.35	106.24	0.28	n20w180s10.2	279.89	72.21	0.33
n20w180s5.3	275.27	33.93	0.25	n20w180s10.3	274.95	106.66	0.23
n20w180s5.4	208.51	41.79	0.40	n20w180s10.4	205.50	97.85	0.30
n20w180s5.5	205.78	930.38	0.43	n20w180s10.5	203.74	1568.37	0.43
n20w200s5.1	238.35	469.75	0.30	n20w200s10.1	238.35	67.87	0.32
n20w200s5.2	220.52	69.06	0.36	n20w200s10.2	216.41	37.70	0.32
n20w200s5.3	250.73	73.05	0.33	n20w200s10.3	250.27	93.48	0.31
n20w200s5.4	299.22	413.12	0.38	n20w200s10.4	298.11	398.81	0.33
n20w200s5.5	243.68	60.14	0.41	n20w200s10.5	236.60	90.19	0.50
Average	247.37	143.67	0.36		243.52	127.58	0.34

MathVNS are compared in problem instances with 20 customers. The model presented in Section 4.2 was solved with CPLEX. Table 6 presents the results of 13 instances out of 50, for which CPLEX was able to provide an upper bound at the end of the 2-h time limit with an optimality gap of 100%. Column 'CPLEX' reports the total cost of the solutions obtained by CPLEX. The best solution found by MathVNS and the average runtime in seconds are presented under the columns 'MathVNS and 't(s)', respectively. The last column reports the percentage improvement of MathVNS over CPLEX. The results show that MathVNS can find significantly better solutions in less than one second on average.

We employed the same experimental setup to also solve the small-size dataset of Schneider et al. (2014) involving a single vehicle under the ETSPTW-BD setting. The CPLEX and MathVNS results are compared in Table 7. The values following 'c' and 's' in the instance name indicate the number of customers and charging stations, respectively. 'TC' columns refer to the total energy consumption and battery degradation cost of the solution obtained by CPLEX and the best solution obtained by MathVNS, respectively. The optimality gap of the solutions found with CPLEX is reported under column '%Gap' in terms of percentage. We see that MathVNS finds the optimal solution in all 5- and 10-customer instances except in r203c10-s5, where it matches the upper bound determined by CPLEX. In the two 15-customer instances, MathVNS outperforms CPLEX significantly in both solution quality (indicated in bold) and computation time.

6.5. Effect of considering battery degradation in route planning

In this section, we investigate the effect of battery degradation on route plans and costs by comparing the solutions of the ETSPTW and ETSPTW-BD found by MathVNS. 25 runs were performed for each instance of the dataset of Roberti and Wen (2016), and the best solutions and average runtimes are reported. Note that the EV is assumed to start its tour with its battery fully charged in the ETSPTW in line with the common approach in the literature.

6.5.1. Results for small-size instances

In this subsection, we compare the solutions obtained for 20-customer instances. Table 8 shows the results. Note that TC values under column 'ETSPTW' are based on the optimal solutions presented in Section 6.4.2 and calculated as the realized costs by taking into account the WC. Column '#R' indicates the number of recharges performed along the tours and column '%Δ' reports the percentage cost saving achieved by solving the ETSPTW-BD as compared to the solution of the ETSPTW.

The results indicate that the route plans constructed by taking into account the battery degradation lead to substantial cost savings up to 10.98%. The average savings are 4.90% and 5.75% in 5- and 10-station instances, respectively. The availability of more stations yields more savings on average. The results also show that incorporating battery degradation in route planning results in more frequent recharges en route. This is an expected result due to the non-decreasing WC function where lower SOC intervals are more preferable. Although the computational times are very short in general, the runtimes rise by 34% and 61% in 5- and 10-station instances, respectively, when the battery degradation is considered. The statistical details of the results are presented in Appendix B.

Table 6
Comparison of ETSPTW-BD results for 20-customer problems.

Instance	CPLEX	MathVNS	t(s)	%Imp
n20w120s5.1	1034.75	1021.63	0.81	1.27
n20w120s5.2	953.90	875.39	0.53	8.23
n20w120s5.5	1395.54	975.21	0.45	30.12
n20w140s5.2	1206.84	1067.26	0.43	11.57
n20w140s5.3	987.54	909.55	0.15	7.90
n20w140s5.4	1254.21	1024.95	0.29	18.28
n20w160s5.3	1087.94	838.45	0.34	22.93
n20w160s5.4	894.95	798.92	0.52	10.73
n20w160s5.5	1127.29	991.81	0.74	12.02
n20w120s10.1	1058.80	1006.83	0.84	4.91
n20w120s10.5	964.52	938.98	0.55	2.65
n20w140s10.1	892.11	697.28	0.42	21.84
n20w140s10.3	1034.07	895.38	0.16	13.41
Average	1068.65	926.28	0.48	12.76

Table 7
Comparison of ETSPTW-BD results for Schneider et al. (2014) small-size problems.

Instance	CPLEX			MathVNS	
	TC	t(s)	%Gap	TC	t(s)
c103c5-s2	656.58	0.17	0.00	656.58	0.04
c206c5-s4	960.03	0.23	0.00	960.03	0.05
c208c5-s3	626.90	0.25	0.00	626.90	0.05
r202c5-s3	517.30	0.64	0.00	517.30	0.04
r203c5-s4	696.69	0.53	0.00	696.69	0.04
rc204c5-s4	713.66	2.52	0.00	713.66	0.04
rc208c5-s3	656.67	0.97	0.00	656.67	0.03
c202c10-s5	1157.38	5.43	0.00	1157.38	0.07
r201c10-s4	942.12	32.29	0.00	942.12	0.08
r203c10-s5	871.55	7200.00	94.91	871.55	0.08
rc201c10-s4	1635.78	0.7	0.00	1635.78	0.07
r209c15-s5	1366.20	7200.00	100.00	**1232.64**	0.28
rc204c15-s7	1700.47	7200.00	100.00	**1475.92**	0.43
Average	961.64	1664.90	22.69	934.09	0.10

6.5.2. Results for large-size instances

We compare the solutions obtained for 150- and 200-customer instances in this subsection. The results are presented in Table 9. Similar to the results obtained in small-size data, total costs improve in all problems. In 5-(10-) station instances, the average saving is 4.08% (5.39%), while it can be up to 6.86% (7.34%). These results also point at higher cost reduction and recharges that are more frequent when more stations are available in the area. On the other hand, incorporating battery degradation brings additional complexity and increases the computational effort by 32% and 35% in the instances with 5- and 10-stations, respectively. Overall, we see that the total delivery costs can be reduced when the recharge frequency, energy amounts, and the visiting sequence of customers are determined efficiently by taking into account the trade-off between energy consumption and the WC by using tailored mechanisms. The statistical details of the results are presented in Appendix B.

6.6. Trade-off analysis

In this section, we perform trade-off analyses to investigate the influence of battery size and time-window lengths on costs by using the subset of instances employed in parameter tuning.

6.6.1. The effect of battery size

We observed in Section 6.5 that the frequency of recharging visits along the tours may increase in the presence of the WC. So, we investigated the impact of bigger size batteries on the solutions by increasing the EV battery capacity by 25% and 50%. The results are summarized in Table 10. In addition to two settings of 'ETSPTW' and 'ETSPTW-BD' whose results are presented in Section 6.5, the results under column 'ETSPTW no-BD cost' report the total cost of energy when WC is neglected, which is linearly proportional to the total distance of the tour. The values in the table show the percentage changes observed in costs resulting from bigger batteries for the three settings separately. A negative value indicates saving.

As battery size increases, the need for energy during the trip

Table 8
Effect of battery degradation on small-size instances.

	ETSPTW			ETSPTW-BD					ETSPTW			ETSPTW-BD			
Instance	TC	t (s)	#R	TC	t (s)	#R	%Δ	Instance	TC	t(s)	#R	TC	t(s)	#R	%Δ
n20w120s5.1	1114.28	0.54	4	1021.63	0.81	6	8.31	n20w120s10.1	1131.02	0.66	3	1006.83	0.84	7	10.98
n20w120s5.2	933.63	0.63	3	875.39	0.53	5	6.24	n20w120s10.2	894.67	0.63	3	843.69	0.76	5	5.70
n20w120s5.3	1205.80	0.29	3	1190.44	0.41	5	1.27	n20w120s10.3	1195.92	0.24	3	1171.81	0.44	6	2.02
n20w120s5.4	1239.07	0.23	4	1175.12	0.42	6	5.16	n20w120s10.4	1208.16	0.53	3	1139.19	0.42	6	5.71
n20w120s5.5	1008.12	0.25	3	975.21	0.45	5	3.26	n20w120s10.5	982.46	0.33	3	938.98	0.55	6	4.43
n20w140s5.1	760.94	0.20	3	710.51	0.19	5	6.63	n20w140s10.1	742.03	0.21	4	697.28	0.42	5	6.03
n20w140s5.2	1130.90	0.27	2	1067.26	0.43	7	5.63	n20w140s10.2	1035.52	0.32	3	1034.69	0.45	4	0.08
n20w140s5.3	972.20	0.13	3	909.55	0.15	6	6.44	n20w140s10.3	955.22	0.16	4	895.38	0.16	8	6.26
n20w140s5.4	1047.96	0.64	3	1024.95	0.29	4	2.20	n20w140s10.4	998.63	0.53	3	974.70	0.32	6	2.40
n20w140s5.5	906.18	0.34	3	868.65	0.26	6	4.14	n20w140s10.5	924.44	0.33	3	850.57	0.34	7	7.99
n20w160s5.1	977.65	0.31	3	924.46	0.56	5	5.44	n20w160s10.1	977.65	0.43	3	914.81	0.69	6	6.43
n20w160s5.2	878.69	0.45	4	848.71	0.39	4	3.41	n20w160s10.2	880.95	0.60	3	828.46	0.59	4	5.96
n20w160s5.3	887.50	0.28	3	838.45	0.34	4	5.53	n20w160s10.3	887.50	0.31	3	815.40	0.37	6	8.12
n20w160s5.4	862.54	0.30	3	798.92	0.52	5	7.38	n20w160s10.4	862.54	0.32	3	798.26	0.54	5	7.45
n20w160s5.5	1043.10	0.60	3	991.81	0.74	4	4.92	n20w160s10.5	999.96	0.50	3	958.17	1.01	6	4.18
n20w180s5.1	1077.01	0.25	3	1000.49	0.45	6	7.10	n20w180s10.1	1029.07	0.24	3	967.15	0.58	7	6.02
n20w180s5.2	1108.33	0.37	3	1065.46	0.57	5	3.87	n20w180s10.2	1127.32	0.39	3	1051.89	0.54	6	6.69
n20w180s5.3	1108.57	0.26	3	1059.81	0.44	5	4.40	n20w180s10.3	1136.74	0.27	4	1046.90	0.56	6	7.90
n20w180s5.4	823.09	0.32	3	788.39	0.55	4	4.22	n20w180s10.4	803.08	0.31	3	768.38	0.73	4	4.32
n20w180s5.5	831.34	0.43	3	798.85	0.75	4	3.91	n20w180s10.5	817.87	0.41	3	780.34	1.06	6	4.59
n20w200s5.1	935.90	0.22	3	924.49	0.45	4	1.22	n20w200s10.1	935.90	0.24	3	897.41	0.72	7	4.11
n20w200s5.2	879.79	0.26	4	839.75	0.47	5	4.55	n20w200s10.2	863.16	0.25	4	815.74	0.53	5	5.49
n20w200s5.3	994.31	0.33	4	953.70	0.43	4	4.08	n20w200s10.3	975.16	0.33	4	928.44	0.77	6	4.79
n20w200s5.4	1239.10	0.42	3	1130.32	0.55	5	8.78	n20w200s10.4	1228.18	0.46	5	1107.15	0.72	7	9.85
n20w200s5.5	969.71	0.47	4	926.50	0.65	6	4.46	n20w200s10.5	971.62	0.50	3	909.83	1.11	7	6.36
Average	997.43	0.35	3.20	948.35	0.47	5	4.90		982.59	0.38	3.28	925.66	0.61	5.92	5.75

decreases, which may result in fewer detours, reduced tour length, hence less energy consumption. MathVNS unsurprisingly achieves cost improvements for all instances in the first and third settings. On the other hand, we observe increased costs in some instances under the second setting (indicated in bold). The reason is that the WC associated with a bigger battery size may outweigh the savings achieved by reduced energy consumption. For example, when the battery size is increased by 50% in instance 'n150w140s5.1', the tour length (hence the energy consumption) reduces by 1.34%, whereas the total cost of the same tour increases by 3.22% due to WC. This example shows that, as opposed to the common conception in the literature, utilizing EVs with bigger batteries does not guarantee to improve the true operational costs obtained using the existing approaches. However, when battery degradation is taken into account (i.e. in the case of ETSPTW-BD), a total saving of 3.17% can be achieved, which offers an even larger saving than the mal-conceived 1.34%. Overall, the average results show that incorporating the battery degradation results in more reduction in total cost through improved route and charge planning: 0.41% (0.57%) compared to 2.32% (3.57%) savings on average with 25% (50%) larger battery.

6.6.2. The effect of time windows

Customer time windows may substantially increase the delivery costs, especially in the presence of WC. To investigate their influence on total costs we repeat our experiments on the ETSPTW-BD by extending customer time-window lengths while keeping the planning horizon the same. We consider two settings, extending the late arrival times by 50% of the corresponding time window length and removing the time window restriction. Table 11 presents the results in comparison to those presented in Section 6.5. 'ΔTC (%)' reports the percentage change in total cost and 'Δ#R' shows the change in the number of recharging visits.

The results show that relaxing time window restrictions can lead to significant reductions in total costs, as expected. Also expected is the need for less frequent recharges due to time flexibility of visiting customers. However, in two instances, 'n150w120s5.2' and 'n200w140s5.4', we see that the EV makes one additional recharging visit when the customer late service times are extended by 50% (indicated in bold). This is not surprising either because the presence of the WC may favor additional recharges with enhanced decisions on energy amounts for achieving improved route plans.

7. Conclusion

In this study, we investigated the influence of battery wear cost on route and charge planning within the context of the ETSPTW. We presented the mathematical model of the problem and developed a math-heuristic algorithm, MathVNS, which couples the VNS algorithm with an exact solver. The performance of MathVNS was validated using TSPTW data from the literature. In addition, MathVNS outperformed CPLEX in terms of solution quality and computational time in small-size ETSPTW and ETSPTW-BD data. Our results on small- and large-size data showed that up to 10.98% and 7.34% cost reduction, respectively, can be realized if battery degradation cost is incorporated in modeling and algorithm development. The average savings is 5% approximately.

Optimizing overnight charging at the depot instead of performing a full charge, which is the common assumption in the literature and practice in the sector, may provide substantial savings in cost due to the effect of battery degradation on operational costs. On the other hand, incorporating battery wear cost in planning may increase the frequency of recharges along the tour, which may bring an additional operational burden for the LSPs. In addition, our trade-off analysis with respect to battery size demonstrated that, as opposed to the common belief in the literature, the use of bigger batteries may increase the actual operational

Table 9
Effect of battery degradation on large-size instances.

	ETSPTW			ETSPTW-BD					ETSPTW			ETSPTW-BD			
Instance	TC	t(s)	#R	TC	t(s)	#R	%Δ	Instance	TC	t (s)	#R	TC	t (s)	#R	%Δ
n150w120s5.1	3163.53	28.36	7	2946.55	31.00	12	6.86	n150w120s10.1	3066.87	28.56	7	2882.64	34.68	14	6.01
n150w120s5.2	2629.22	21.92	6	2519.96	39.12	9	4.16	n150w120s10.2	2619.78	21.88	6	2472.51	39.00	11	5.62
n150w120s5.3	3186.59	18.24	8	3176.46	19.44	8	0.32	n150w120s10.3	3173.32	18.96	8	3156.89	21.16	11	0.52
n150w120s5.4	2791.63	23.28	7	2704.49	29.20	9	3.12	n150w120s10.4	2809.94	23.04	6	2632.86	30.40	13	6.30
n150w120s5.5	2892.34	21.56	9	2763.56	40.84	13	4.45	n150w120s10.5	2844.28	20.92	8	2635.41	41.12	15	7.34
n150w140s5.1	3048.80	30.44	8	2917.76	41.00	11	4.30	n150w140s10.1	3049.03	29.88	8	2845.26	41.24	14	6.68
n150w140s5.2	3100.06	21.96	8	2986.48	37.64	12	3.66	n150w140s10.2	3096.72	22.00	7	2917.03	37.72	13	5.80
n150w140s5.3	2547.36	23.28	7	2434.18	39.56	11	4.44	n150w140s10.3	2544.59	23.76	8	2403.06	50.88	12	5.56
n150w140s5.4	2758.18	17.32	8	2630.78	25.40	13	4.62	n150w140s10.4	2747.57	17.32	8	2580.90	23.00	16	6.07
n150w140s5.5	2622.80	30.80	7	2545.28	38.16	11	2.96	n150w140s10.5	2580.34	30.76	7	2474.20	37.96	14	4.11
n150w160s5.1	3026.75	22.68	7	2819.10	27.84	10	6.86	n150w160s10.1	2929.22	21.96	7	2749.64	36.04	14	6.13
n150w160s5.2	2920.03	31.48	7	2832.41	41.20	11	3.00	n150w160s10.2	2849.93	31.64	7	2739.07	41.24	10	3.89
n150w160s5.3	2418.35	18.32	7	2376.24	25.84	10	1.74	n150w160s10.3	2412.05	18.56	7	2317.31	26.84	11	3.93
n150w160s5.4	2785.13	23.40	7	2700.12	25.48	10	3.05	n150w160s10.4	2808.89	23.44	7	2648.12	25.00	15	5.72
n150w160s5.5	2781.62	27.28	7	2629.97	43.44	12	5.45	n150w160s10.5	2678.73	27.08	8	2564.83	46.96	10	4.25
n200w120s5.1	2997.13	53.28	6	2882.18	94.40	8	3.84	n200w120s10.1	3032.07	52.52	6	2822.28	94.00	10	6.92
n200w120s5.2	3059.62	62.24	9	2894.23	72.08	12	5.41	n200w120s10.2	2998.27	62.24	9	2831.05	73.56	14	5.58
n200w120s5.3	3429.22	62.24	8	3282.02	78.64	12	4.29	n200w120s10.3	3371.26	62.36	8	3184.87	79.24	13	5.53
n200w120s5.4	3391.19	62.00	7	3234.27	65.76	11	4.63	n200w120s10.4	3344.27	62.00	8	3126.69	64.04	14	6.51
n200w120s5.5	3278.67	53.48	7	3135.87	71.36	10	4.36	n200w120s10.5	3207.94	53.52	8	3052.36	58.08	15	4.85
n200w140s5.1	3299.12	85.92	7	3146.56	102.96	10	4.62	n200w140s10.1	3290.84	86.00	7	3094.30	102.36	13	5.97
n200w140s5.2	3243.97	73.48	8	3121.76	96.44	12	3.77	n200w140s10.2	3211.71	71.48	7	3057.77	99.80	12	4.79
n200w140s5.3	2988.91	53.48	8	2852.66	63.40	11	4.56	n200w140s10.3	2930.87	53.52	9	2811.51	66.44	12	4.07
n200w140s5.4	3120.22	83.88	8	2977.19	107.20	10	4.58	n200w140s10.4	3162.53	83.84	8	2960.55	112.64	12	6.39
n200w140s5.5	3304.51	54.76	8	3204.75	73.68	11	3.02	n200w140s10.5	3377.51	54.84	7	3164.25	75.96	12	6.31
Average	2991.40	40.20	7.44	2868.60	53.24	10.76	4.08		2965.54	40.08	7.44	2805.01	54.37	12.80	5.39

Table 10
Percentage changes in cost for different battery sizes.

	25% Larger Battery			50% Larger Battery		
Instance	ETSPTW no-BD	ETSPTW	ETSPTW-BD	ETSPTW no-BD	ETSPTW	ETSPTW-BD
n150w120s5.2	−1.69	**0.14**	−1.96	−2.67	−2.34	−2.87
n150w140s5.1	−0.82	**1.32**	−2.02	−1.34	**3.22**	−3.17
n150w140s5.4	−0.14	−0.73	−1.96	−0.52	**1.49**	−2.86
n150w160s5.2	−3.10	−3.90	−4.84	−3.49	−4.01	−7.00
n150w160s5.3	−0.01	−0.79	−3.58	−0.60	**1.76**	−5.03
n200w120s5.1	−1.60	**0.82**	−2.10	−2.05	**0.14**	−3.28
n200w120s5.4	−0.48	−3.05	−1.98	−0.74	−3.30	−3.53
n200w120s5.5	−0.66	**1.50**	−1.49	−0.66	−0.93	−2.40
n200w140s5.3	−1.11	−0.57	−1.67	−1.12	−0.43	−2.84
n200w140s5.4	−0.25	**1.24**	−1.63	−0.25	−1.30	−2.67
Average	−1.00	−0.41	−2.32	−1.34	−0.57	−3.57

Table 11
Comparisons of results for extended time windows.

	50%		No TW	
Instance	ΔTC (%)	Δ#R	ΔTC (%)	Δ#R
n150w120s5.2	−2.58	**1**	−32.00	−5
n150w140s5.1	−7.23	**-**	−39.87	−6
n150w140s5.4	−3.07	−1	−33.24	−7
n150w160s5.2	−11.28	−2	−37.33	−6
n150w160s5.3	−2.78	**-**	−25.04	−5
n200w120s5.1	−7.39	**-**	−28.89	−4
n200w120s5.4	−8.26	−1	−38.46	−6
n200w120s5.5	−7.62	−1	−36.18	−6
n200w140s5.3	−6.68	−1	−29.95	−6
n200w140s5.4	−7.65	**1**	−33.68	−4
Average	−6.45	−0.4	−33.46	−5.5

costs because of their increased wear cost, and battery degradation should be properly incorporated in the problem in order to really benefit from the additional battery capacity.

Future research on this topic may focus on tackling the EVRP variants by considering battery degradation. Since EVRP involves an EV fleet whose size might be large, it offers more potential for cost reduction. On the other hand, the problem complexity will increase significantly in the presence of wear cost, and effective algorithms are needed to solve the problem in reasonable time. In addition, the impact of charging power on battery wear in the cases of fast- and super-fast technologies can be investigated to improve the related charging decisions. Finally, the effect of non-increasing and custom wear cost functions can also be investigated in devising route plans.

Unlisted references

EU, 2022; Kancharla and Ramaduari, 2020; Rastani and Çatay, 2021; EIA, 2022; .

CRediT authorship contribution statement

Raci Berk İslim: Conceptualization, Data curation, Formal analysis, Investigation, Methodology, Validation, Visualization, Writing – original draft, Writing – review & editing. **Bülent Çatay:** Conceptualization, Formal analysis, Investigation, Methodology, Supervision, Validation, Writing – original draft, Writing – review & editing, Visualization.

Declaration of competing interest

The authors declare that they have no known competing financial interests or personal relationships that could have appeared to influence the work reported in this paper.

Data availability

The data has been shared with a web link.

Acknowledgements

The authors thank all the anonymous referees for their valuable comments and suggestions that helped improve the overall quality of the paper.

Appendix A. Data modification procedure

Rounding down the Euclidean distances to integer values may violate the triangular property and yield unrealistic, even infeasible in the presence of time windows, solutions. Therefore, we used two decimal-place precision and truncated the Euclidean distance between each pair of nodes from the hundredths place. Since the tour lengths increase with higher precision, we extend the length of the planning horizon and late arrival times of customer nodes in the data proportionally to maintain the feasibility of the original data.

Table A.1
Data modification

Small-size data				Large-size data			
Instance	Integer	2-Decimal	%Δ	Instance	Integer	2-Decimal	%Δ
n20w120.1	267	280.74	5.15	n150w120.1	734	786.51	7.15
n20w120.2	218	225.92	3.63	n150w120.2	677	727.89	7.52
n20w120.3	303	310.25	2.39	n150w120.3	747	787.96	5.48
n20w120.4	300	309.33	3.11	n150w120.4	763	812.89	6.54
n20w120.5	240	246.61	2.75	n150w120.5	689	734.42	6.59

(*continued on next page*)

Table A.1 (*continued*)

Small-size data				Large-size data			
Instance	Integer	2-Decimal	%Δ	Instance	Integer	2-Decimal	%Δ
n20w140.1	176	184.94	5.08	n150w140.1	762	811.4	6.48
n20w140.2	272	280.31	3.06	n150w140.2	755	807.72	6.98
n20w140.3	236	241.97	2.53	n150w140.3	613	670.93	9.45
n20w140.4	255	258.54	1.39	n150w140.4	676	717.49	6.14
n20w140.5	225	228.52	1.56	n150w140.5	663	709.88	7.07
n20w160.1	241	250.82	4.07	n150w160.1	706	752.93	6.65
n20w160.2	201	207.77	3.37	n150w160.2	711	756.38	6.38
n20w160.3	201	206.62	2.80	n150w160.3	608	659.79	8.52
n20w160.4	203	209.21	3.06	n150w160.4	672	712.69	6.06
n20w160.5	245	252.93	3.24	n150w160.5	658	705.56	7.23
n20w180.1	253	260.47	2.95	n200w120.1	799	918.05	14.90
n20w180.2	265	273.93	3.37	n200w120.2	721	774.13	7.37
n20w180.3	271	278.87	2.90	n200w120.3	880	939.96	6.81
n20w180.4	201	218.22	8.57	n200w120.4	777	836.96	7.72
n20w180.5	193	199.04	3.13	n200w120.5	841	905.15	7.63
n20w200.1	233	239.74	2.89	n200w140.1	834	904.68	8.47
n20w200.2	203	208.25	2.59	n200w140.2	760	819.19	7.79
n20w200.3	249	257.04	3.23	n200w140.3	758	821.27	8.35
n20w200.4	293	297.85	1.66	n200w140.4	816	903.21	10.69
n20w200.5	227	231.59	2.02	n200w140.5	822	882.23	7.33

Table A.1 reports the increase in the TSPTW tour lengths when the Euclidean distances are truncated to two decimal places instead of rounded down to the nearest integer. The first column shows the nomenclature of the instances. The column under 'Integer' reports the length of the best-known tours reported in the literature, while the column under '2-Decimal' presents the best tours determined by MathVNS using two decimal-place precision data. The reason why we did not use the tours presented in the literature by recalculating their lengths with the updated distance values is two-fold: (i) some of the best tours reported in the literature violate the time window restrictions; and (ii) MathVNS was able to find shorter tours in some instances. The increase in the length of the tours is reported under column '%Δ', which is used to extend the time windows.

Appendix B. Statistical analyses of results

The detailed results of our experimental study presented in Section 6.5 are shown in Table B.1 and B.2. Columns 'Best' and 'Average' report the best and average solutions obtained over 25 runs, respectively. The coefficient of variation of the solutions are displayed under 'CoV' column.

Table B.1
Detailed results for small-size instances

Instance	Best	Average	CoV	Instance	Best	Average	CoV
n20w120s5.1	1021.63	1021.63	0.000	n20w120s10.1	1006.83	1006.83	0.000
n20w120s5.2	875.39	883.09	0.023	n20w120s10.2	843.69	852.16	0.024
n20w120s5.3	1190.44	1192.98	0.007	n20w120s10.3	1171.81	1171.88	0.000
n20w120s5.4	1175.12	1175.12	0.000	n20w120s10.4	1139.19	1139.19	0.000
n20w120s5.5	975.21	975.21	0.000	n20w120s10.5	938.98	938.98	0.000
n20w140s5.1	710.51	710.51	0.000	n20w140s10.1	697.28	697.28	0.000
n20w140s5.2	1067.26	1098.27	0.011	n20w140s10.2	1034.69	1076.50	0.018
n20w140s5.3	909.55	909.55	0.000	n20w140s10.3	895.38	895.38	0.000
n20w140s5.4	1024.95	1051.69	0.010	n20w140s10.4	974.70	974.70	0.000
n20w140s5.5	868.65	868.65	0.000	n20w140s10.5	850.57	850.57	0.000
n20w160s5.1	924.46	924.46	0.000	n20w160s10.1	914.81	914.81	0.000
n20w160s5.2	848.71	848.71	0.000	n20w160s10.2	828.46	828.46	0.000
n20w160s5.3	838.45	838.45	0.000	n20w160s10.3	815.40	815.40	0.000
n20w160s5.4	798.92	810.59	0.016	n20w160s10.4	798.26	809.87	0.017
n20w160s5.5	991.81	1012.33	0.011	n20w160s10.5	958.17	963.17	0.003
n20w180s5.1	1000.49	1000.49	0.000	n20w180s10.1	967.15	967.15	0.000
n20w180s5.2	1065.46	1072.26	0.014	n20w180s10.2	1051.89	1054.04	0.005
n20w180s5.3	1059.81	1073.33	0.013	n20w180s10.3	1046.90	1061.98	0.009
n20w180s5.4	788.39	788.39	0.000	n20w180s10.4	768.38	768.38	0.000
n20w180s5.5	798.85	798.85	0.000	n20w180s10.5	780.34	781.43	0.001
n20w200s5.1	924.49	924.49	0.000	n20w200s10.1	897.41	897.41	0.000

(*continued on next page*)

Table B.1 (*continued*)

Instance	Best	Average	CoV	Instance	Best	Average	CoV
n20w200s5.2	839.75	839.75	0.000	n20w200s10.2	815.74	815.74	0.000
n20w200s5.3	953.70	960.27	0.001	n20w200s10.3	928.44	928.44	0.000
n20w200s5.4	1130.32	1197.86	0.038	n20w200s10.4	1107.15	1155.42	0.032
n20w200s5.5	926.50	973.51	0.029	n20w200s10.5	909.83	920.33	0.006

Table B.2
Detailed results for large-size instances

Instance	Best	Average	CoV	Instance	Best	Average	CoV
n150w120s5.1	2946.55	3026.92	0.021	n150w120s10.1	2882.64	2944.86	0.018
n150w120s5.2	2519.96	2580.61	0.013	n150w120s10.2	2472.51	2518.49	0.009
n150w120s5.3	3176.46	3180.66	0.003	n150w120s10.3	3156.89	3160.53	0.002
n150w120s5.4	2704.49	2740.96	0.014	n150w120s10.4	2632.86	2670.27	0.016
n150w120s5.5	2763.56	2799.74	0.010	n150w120s10.5	2635.41	2680.71	0.016
n150w140s5.1	2917.76	2958.63	0.024	n150w140s10.1	2845.26	2902.06	0.023
n150w140s5.2	2986.48	3093.56	0.026	n150w140s10.2	2917.03	3023.22	0.027
n150w140s5.3	2434.18	2481.00	0.013	n150w140s10.3	2403.06	2441.31	0.011
n150w140s5.4	2630.78	2674.19	0.022	n150w140s10.4	2580.90	2612.31	0.020
n150w140s5.5	2545.28	2609.20	0.014	n150w140s10.5	2474.20	2532.33	0.017
n150w160s5.1	2819.10	2897.34	0.019	n150w160s10.1	2749.64	2831.48	0.016
n150w160s5.2	2832.41	2954.21	0.036	n150w160s10.2	2739.07	2896.63	0.037
n150w160s5.3	2376.24	2399.40	0.010	n150w160s10.3	2317.31	2339.08	0.006
n150w160s5.4	2700.12	2786.16	0.024	n150w160s10.4	2648.12	2740.29	0.023
n150w160s5.5	2629.97	2716.95	0.017	n150w160s10.5	2564.83	2670.26	0.024
n200w120s5.1	2882.18	3048.46	0.049	n200w120s10.1	2822.28	2978.23	0.047
n200w120s5.2	2894.23	2951.86	0.016	n200w120s10.2	2831.05	2884.23	0.012
n200w120s5.3	3282.02	3351.77	0.018	n200w120s10.3	3184.87	3283.37	0.019
n200w120s5.4	3234.27	3276.80	0.015	n200w120s10.4	3126.69	3165.90	0.016
n200w120s5.5	3135.87	3177.92	0.014	n200w120s10.5	3052.36	3077.98	0.012
n200w140s5.1	3146.56	3274.68	0.027	n200w140s10.1	3094.30	3240.56	0.031
n200w140s5.2	3121.76	3257.40	0.025	n200w140s10.2	3057.77	3165.09	0.027
n200w140s5.3	2852.66	3025.34	0.026	n200w140s10.3	2811.51	2984.60	0.023
n200w140s5.4	2977.19	3108.29	0.024	n200w140s10.4	2960.55	3071.69	0.021
n200w140s5.5	3204.75	3279.94	0.020	n200w140s10.5	3164.25	3231.49	0.020

We investigated the influence of the value of *Slack* on the solution quality by setting it equal to 0% (i.e. no slack) and 2% (i.e. extended slack), and repeating our experiments on all large-size instances. We performed Friedman's test, whose null hypothesis states that *Slack* value does not affect the solutions. Our tests based on the average and best solutions out of 25 runs resulted in *p*-values of 0.003 and 0.095, respectively. These results indicate that there exists a statistically significant difference between the average solutions, whereas the difference between the best solutions is not statistically significant with 95% confidence level.

We also performed Wilcoxon signed-rank tests to make pairwise statistical analyses. The *p*-values are given in Table B.3. Based on the best solutions obtained using *Slack* values of 0% and 1%, our test revealed a significant difference in favor of 1% ($p = 0.003$). Likewise, the best solutions obtained with *Slack* = 1 % are significantly better than those obtained with *Slack* = 2 % ($p = 0.993$). The *p*-values associated with tests on average solutions point to similar results. We, therefore, conclude that the *Slack* mechanism enhances the performance of MathVNS and the solutions obtained with *Slack* = 1% (i.e. the parameter value used in our experiments) outperform those obtained by using values of 0% and 2%.

Table B.3
p-values obtained with Wilcoxon signed-rank test

	Best Solutions		Average Solutions	
Slack	1%	2%	1%	2%
0%	0.003	0.105	0.000	0.000
1%	–	0.993	–	0.284

References

Almouhanna, A., Quintero-Araujo, C.L., Panadero, J., Juan, A.A., Khosravi, B., Ouelhadj, D., 2020. The location routing problem using electric vehicles with constrained distance. Comput. Oper. Res. 115, 104864 https://doi.org/10.1016/j.cor.2019.104864.

Amiri, A., Zolfagharinia, H., Amin, S.H., 2023. A robust multi-objective routing problem for heavy-duty electric trucks with uncertain energy consumption. Comput. Ind. Eng. 178, 109108 https://doi.org/10.1016/j.cie.2023.109108.

Azadeh, S.S., Vester, J., Maknoon, M.Y., 2022. Electrification of a bus system with fast charging stations: impact of battery degradation on design decisions. Transport. Res. C Emerg. Technol. 142, 103807 https://doi.org/10.1016/j.trc.2022.103807.
Barco, J., Guerra, A., Muñoz, L., Quijano, N., 2017. Optimal routing and scheduling of charge for electric vehicles: a case study. Math. Probl Eng. 2017 https://doi.org/10.1155/2017/8509783.
Barré, A., Deguilhem, B., Grolleau, S., Gérard, M., Suard, F., Riu, D., 2013. A review on lithium-ion battery ageing mechanisms and estimations for automotive applications. J. Power Sources 241, 680–689. https://doi.org/10.1016/j.jpowsour.2013.05.040.
Breunig, U., Baldacci, R., Hartl, R.F., Vidal, T., 2019. The electric two-echelon vehicle routing problem. Comput. Oper. Res. 103, 198–210. https://doi.org/10.1016/j.cor.2018.11.005.
Comert, S.E., Yazgan, H.R., 2023. A new approach based on hybrid ant colony optimization-artificial bee colony algorithm for multi-objective electric vehicle routing problems. Eng. Appl. Artif. Intell. 123, 106375 https://doi.org/10.1016/j.engappai.2023.106375.
Council of the European Union, 2022. Fit for 55 package: council reaches general approaches relating to emissions reductions and their social impacts. Press release. https://www.consilium.europa.eu/en/press/press-releases/2022/06/29/fit-for-55-council-reaches-general-approaches-relating-to-emissions-reductions-and-removals-and-their-social-impacts/.
da Silva, R.F., Urrutia, S., 2010. A general VNS heuristic for the traveling salesman problem with time windows. Discrete Optim. 7 (4), 203–211. https://doi.org/10.1016/j.disopt.2010.04.002.
de Armas, J., Melian-Batista, B., Moreno-Perez, J.A., Brito, J., 2015. GVNS for a real-world rich vehicle routing problem with time windows. Eng. Appl. Artif. Intell. 42, 45–56. https://doi.org/10.1016/j.engappai.2015.03.009.
Dempsey, H., 2022. Electric car battery prices rise for first time in more than a decade. December 6 Financ. Times. Retrieved from. https://www.ft.com/content/f6c409d3-a29b-48f8-9f17-5586a1963d16#.
DHL, 2022. How DHL is embracing electric vehicles (EVs) for a greener, sustainable future. Retrieved from. https://www.dhl.com/discover/en-sg/logistics-advice/sustainability-and-green-logistics/reasons-dhl-embraces-electric-vehicles.
Doppstadt, C., Koberstein, A., Vigo, D., 2020. The hybrid electric vehicle traveling salesman problem with time windows. Eur. J. Oper. Res. 284 (2), 675–692. https://doi.org/10.1016/j.ejor.2019.12.031.
Erdelić, T., Carić, T., 2019. A survey on the electric vehicle routing problem: variants and solution approaches. J. Adv. Transport. 2019 https://doi.org/10.1155/2019/5075671.
Erdoğan, S., Miller-Hooks, E., 2012. A green vehicle routing problem. Transport. Res. E Logist. Transport. Rev. 48 (1), 100–114. https://doi.org/10.1016/j.tre.2011.08.001.
Felipe, Á., Ortuño, M.T., Righini, G., Tirado, G., 2014. A heuristic approach for the green vehicle routing problem with multiple technologies and partial recharges. Transport. Res. E Logist. Transport. Rev. 71, 111–128. https://doi.org/10.1016/j.tre.2014.09.003.
Feng, W., Figliozzi, M., 2013. An economic and technological analysis of the key fac-tors affecting the competitiveness of electric commercial vehicles: a case study from the USA market. Transport. Res. C Emerg. Technol. 26, 135–145. https://doi.org/10.1016/j.trc.2012.06.007.
Fleming, C.L., Griffis, S.E., Bell, J.E., 2013. The effects of triangle inequality on the vehicle routing problem. Eur. J. Oper. Res. 224 (1), 1–7. https://doi.org/10.1016/j.ejor.2012.07.005.
Froger, A., Mendoza, J.E., Jabali, O., Laporte, G., 2019. Improved formulations and algorithmic components for the electric vehicle routing problem with nonlinear charging functions. Comput. Oper. Res. 104, 256–294. https://doi.org/10.1016/j.cor.2018.12.013.
Goeke, D., Schneider, M., 2015. Routing a mixed fleet of electric and conventional vehicles. Eur. J. Oper. Res. 245 (1), 81–99. https://doi.org/10.1016/j.ejor.2015.01.049.
Guo, F., Zhang, J., Huang, Z., Huang, W., 2022. Simultaneous charging station location-routing problem for electric vehicles: effect of nonlinear partial charging and battery degradation. Energy 250, 123724. https://doi.org/10.1016/j.energy.2022.123724.
Han, S., Han, S., Aki, H., 2014. A practical battery wear model for electric vehicle charging applications. Appl. Energy 113, 1100–1108. https://doi.org/10.1016/j.apenergy.2013.08.062.
Hansen, P., Mladenović, N., Brimberg, J., Peréz, A.M., 2010. Variable neighborhood search, 2010. In: Gendreau, M., Potvin, J.Y. (Eds.), Handbook of Metaheuristics. Springer, New York, pp. 61–86. https://doi.org/10.1007/978-1-4419-1665-5.
Hof, J., Schneider, M., Goeke, D., 2017. Solving the battery swap station location-routing problem with capacitated electric vehicles using an AVNS algorithm for vehicle-routing problems with intermediate stops. Transp. Res. Part B Methodol. 97, 102–112. https://doi.org/10.1016/j.trb.2016.11.009.
International Energy Agency, 2022. CO2 emissions by sector, world 1990-2019. Retrieved from. https://www.iea.org/data-and-statistics/data-browser?country=WORLD&fuel=CO2%20emissions&indicator=CO2BySector.
İslim, R.B., Çatay, B., 2022. The effect of battery degradation on the route optimization of electric vehicles. Proc. Comput. Sci. 204, 1–8. https://doi.org/10.1016/j.procs.2022.08.118.
Jin, H., 2022. Analysis: Ukraine invasion sets back Musk's dream for cheaper EVs, for now. Reuters. Retrieved from: https://www.reuters.com/technology/ukraine-invasion-sets-back-musks-dream-cheaper-evs-now-2022-03-07/. .
Kancharla, S.R., Ramadurai, G., 2020. Electric vehicle routing problem with non-linear charging and load-dependent discharging. Expert Syst. Appl. 160, 113714 https://doi.org/10.1016/j.eswa.2020.113714.
Keskin, M., Çatay, B., 2016. Partial recharge strategies for the electric vehicle routing problem with time windows. Transport. Res. C Emerg. Technol. 65, 111–127. https://doi.org/10.1016/j.trc.2016.01.013.
Keskin, M., Çatay, B., 2018. A matheuristic method for the electric vehicle routing problem with time windows and fast chargers. Comput. Oper. Res. 100, 172–188. https://doi.org/10.1016/j.cor.2018.06.019.
Keskin, M., Çatay, B., Laporte, G., 2021. A simulation-based heuristic for the electric vehicle routing problem with time windows and stochastic waiting times at recharging stations. Comput. Oper. Res. 125, 105060 https://doi.org/10.1016/j.cor.2020.105060.
Keskin, M., Laporte, G., Çatay, B., 2019. Electric vehicle routing problem with time-dependent waiting times at recharging stations. Comput. Oper. Res. 107, 77–94. https://doi.org/10.1016/j.cor.2019.02.014.
König, A., Nicoletti, L., Schröder, D., Wolff, S., Waclaw, A., Lienkamp, M., 2021. An overview of parameter and cost for battery electric vehicles. World Electric Vehicle Journal 12 (1), 21. https://doi.org/10.3390/wevj12010021.
Kullman, N.D., Goodson, J., Mendoza, J.E., 2018. Dynamic electric vehicle routing with mid-route recharging and uncertain availability. In: ODYSSEUS 2018. Retrieved from: https://hal.science/hal-01814644/document.
Küçükoğlu, I., Dewil, R., Cattrysse, D., 2021. The electric vehicle routing problem and its variations: a literature review. Comput. Ind. Eng. 161, 107650 https://doi.org/10.1016/j.cie.2021.107650.
Lin, B., Ghaddar, B., Nathwani, J., 2021. Electric vehicle routing with charging/discharging under time-variant electricity prices. Transport. Res. C Emerg. Technol. 130, 103285 https://doi.org/10.1016/j.trc.2021.103285.
Lu, J., Chen, Y., Hao, J.K., He, R., 2020. The time-dependent electric vehicle routing problem: model and solution. Expert Syst. Appl. 161, 113593 https://doi.org/10.1016/j.eswa.2020.113593.
Mladenović, N., Hansen, P., 1997. Variable neighborhood search. Comput. Oper. Res. 24 (11), 1097–1100. https://doi.org/10.1016/s0305-0548(97)00031-2.
Mladenović, N., Todosijević, R., Urošević, D., 2012. An efficient GVNS for solving traveling salesman problem with time windows. Electron. Notes Discrete Math. 39, 83–90. https://doi.org/10.1016/j.endm.2012.10.012.
Molina, J.C., Salmeron, J.L., Eguia, I., Racero, J., 2020. The heterogeneous vehicle routing problem with time windows and a limited number of resources. Eng. Appl. Artif. Intell. 94, 103745 https://doi.org/10.1016/j.engappai.2020.103745.
Montoya, A., Guéret, C., Mendoza, J.E., Villegas, J.G., 2017. The electric vehicle routing problem with nonlinear charging function. Transp. Res. Part B Methodol. 103, 87–110. https://doi.org/10.1016/j.trb.2017.02.004.
Ohlmann, J.W., Thomas, B.W., 2007. A compressed-annealing heuristic for the traveling salesman problem with time windows. Inf. J. Comput. 19 (1), 80–90. https://doi.org/10.1287/ijoc.1050.0145.
Pelletier, S., Jabali, O., Laporte, G., 2016. 50th anniversary invited article - goods distribution with electric vehicles: review and research perspectives. Transport. Sci. 50 (1), 3–22. https://doi.org/10.1287/trsc.2015.0646.
Pelletier, S., Jabali, O., Laporte, G., 2018. Charge scheduling for electric freight vehicles. Transp. Res. Part B Methodol. 115, 246–269. https://doi.org/10.1016/j.trb.2018.07.010.
Pelletier, S., Jabali, O., Laporte, G., Veneroni, M., 2017. Battery degradation and behaviour for electric vehicles: review and numerical analyses of several models. Transp. Res. Part B Methodol. 103, 158–187. https://doi.org/10.1016/j.trb.2017.01.020.
Raeesi, R., Zografos, K.G., 2020. The electric vehicle routing problem with time windows and synchronised mobile battery swapping. Transp. Res. Part B Methodol. 140, 101–129. https://doi.org/10.1016/j.trb.2020.06.012.
Rastani, S., Çatay, B., 2021. A large neighborhood search-based matheuristic for the load-dependent electric vehicle routing problem with time windows. Ann. Oper. Res. 1–33. https://doi.org/10.1007/s10479-021-04320-9.
Rastani, S., Yüksel, T., Çatay, B., 2019. Effects of ambient temperature on the route planning of electric freight vehicles. Transport. Res. Transport Environ. 74, 124–141. https://doi.org/10.1016/j.trd.2019.07.025.
Roberti, R., Wen, M., 2016. The electric traveling salesman problem with time windows. Transport. Res. E Logist. Transport. Rev. 89, 32–52. https://doi.org/10.1016/j.tre.2016.01.010.
Rohrbeck, B., Berthold, K., Hettich, F., 2018. Location planning of charging stations for electric city buses considering battery ageing effects. Operations Research Proceedings 701–707. https://doi.org/10.1007/978-3-319-89920-6_93.
Sadati, M.E.H., Akbari, V., Çatay, B., 2022. Electric vehicle routing problem with flexible deliveries. Int. J. Prod. Res. 60 (13), 4268–4294. https://doi.org/10.1080/00207543.2022.2032451.
Saner, C.B., Trivedi, A., Srinivasan, D., 2022. A MILP-based approach to account for battery degradation in electric bus charging scheduling. In: 2022 IEEE PES 14th Asia-Pacific Power and Energy Engineering Conference (APPEEC). IEEE, pp. 1–6. https://doi.org/10.1109/APPEEC53445.2022.10072240.
Sassi, O., Cherif, W.R., Oulamara, A., 2014. Vehicle routing problem with mixed fleet of conventional and heterogenous electric vehicles and time dependent charging costs. Technical Report. https://hal.archives-ouvertes.fr/hal-01083966/document.
Schiffer, M., Walther, G., 2017. The electric location routing problem with time windows and partial recharging. Eur. J. Oper. Res. 260 (3), 995–1013. https://doi.org/10.1016/j.ejor.2017.01.011.
Schiffer, M., Klein, P.S., Laporte, G., Walther, G., 2021. Integrated planning for electric commercial vehicle fleets: a case study for retail mid-haul logistics networks. Eur. J. Oper. Res. 291 (3), 944–960. https://doi.org/10.1016/j.ejor.2020.09.054.
Schneider, M., Stenger, A., Goeke, D., 2014. The electric vehicle routing problem with time windows and recharging stations. Transport. Sci. 48 (4), 500–520. https://doi.org/10.1287/trsc.2013.0490.

Seyfi, M., Alinaghian, M., Ghorbani, E., Çatay, B., Sabbagh, M.S., 2022. Multi-mode hybrid electric vehicle routing problem. Transport. Res. E Logist. Transport. Rev. 166, 102882 https://doi.org/10.1016/j.tre.2022.102882.

Shehabeldeen, A., Foda, A., Mohamed, M., 2023. The impacts of battery capacity degradation on optimizing BEBS transit system configuration. In: 2023 IEEE Transportation Electrification Conference & Expo (ITEC). IEEE, pp. 1–6. https://doi.org/10.1109/ITEC55900.2023.10186983.

Shi, Y., Zhou, Y., Boudouh, T., Grunder, O., 2020. A lexicographic-based two-stage algorithm for vehicle routing problem with simultaneous pickup–delivery and time window. Eng. Appl. Artif. Intell. 95, 103901 https://doi.org/10.1016/j.engappai.2020.103901.

Suzuki, Y., 2014. A variable-reduction technique for the fixed-route vehicle-refueling problem. Comput. Ind. Eng. 67, 204–215. https://doi.org/10.1016/j.cie.2013.11.007.

Sweda, T.M., Dolinskaya, I.S., Klabjan, D., 2017. Adaptive routing and recharging policies for electric vehicles. Transport. Sci. 51 (4), 1326–1348. https://doi.org/10.1287/trsc.2016.0724.

Taş, D., 2021. Electric vehicle routing with flexible time windows: a column generation solution approach. Transportation Letters 13 (2), 97–103. https://doi.org/10.1080/19427867.2020.1711581.

Timilsina, L., Badr, P.R., Hoang, P.H., Ozkan, G., Papari, B., Edrington, C.S., 2023. Battery degradation in electric and hybrid electric vehicles: a survey study. IEEE Access 11, 42431–42462. https://doi.org/10.1109/ACCESS.2023.3271287.

U.S. Energy Information Administration (EIA), 2022. Table 5.3. Average Price of Electricity to Ultimate Customers. Retrieved from. https://www.eia.gov/electricity/monthly/epm_table_grapher.php?t=epmt_5_3.

Vermeer, W., Mouli, G.R.C., Bauer, P., 2022. A comprehensive review on the characteristics and modeling of lithium-ion battery aging. IEEE Transactions on Transportation Electrification 8 (2), 2205–2232. https://doi.org/10.1109/TTE.2021.3138357.

Walmart, 2022. Walmart to Purchase 4,500 Canoo Electric Delivery Vehicles to Be Used for Last Mile Deliveries in Support of its Growing eCommerce Business. Retrieved from. https://corporate.walmart.com/newsroom/2022/07/12/walmart-to-purchase-4-500-canoo-electric-delivery-vehicles-to-be-used-for-last-mile-deliveries-in-support-of-its-growing-ecommerce-business.

Wang, J., Kang, L., Liu, Y., 2020. Optimal scheduling for electric bus fleets based on dynamic programming approach by considering battery capacity fade. Renew. Sustain. Energy Rev. 130, 109978 https://doi.org/10.1016/j.rser.2020.109978.

Wang, L., Gao, S., Wang, K., Li, T., Li, L., Chen, Z., 2020. Time-dependent electric vehicle routing problem with time windows and path flexibility. J. Adv. Transport. 2020, 1–19. https://doi.org/10.1155/2020/3030197.

Xiong, R., Li, L., Tian, J., 2018. Towards a smarter battery management system: a critical review on battery state of health monitoring methods. J. Power Sources 405, 18–29. https://doi.org/10.1016/j.jpowsour.2018.10.019.

Xu, M., Wu, T., Tan, Z., 2021. Electric vehicle fleet size for carsharing services considering on-demand charging strategy and battery degradation. Transport. Res. C Emerg. Technol. 127, 103146 https://doi.org/10.1016/j.trc.2021.103146.

Yang, J., Sun, H., 2015. Battery swap station location-routing problem with capacitated electric vehicles. Comput. Oper. Res. 55, 217–232. https://doi.org/10.1016/j.cor.2014.07.003.

Zang, Y., Wang, M., Qi, H., 2022. A column generation tailored to electric vehicle routing problem with nonlinear battery depreciation. Comput. Oper. Res. 13, 105527 https://doi.org/10.1016/j.cor.2021.105527.

Zeng, Z., Wang, S., Qu, X., 2022. On the role of battery degradation in en-route charge scheduling for an electric bus system. Transport. Res. E Logist. Transport. Rev. 161, 102727 https://doi.org/10.1016/j.tre.2022.102727.

Zhang, L., Wang, S., Qu, X., 2021a. Optimal electric bus fleet scheduling considering battery degradation and non-linear charging profile. Transport. Res. E Logist. Transport. Rev. 154, 102445 https://doi.org/10.1016/j.tre.2021.102445.

Zhang, L., Zeng, Z., Qu, X., 2021b. On the role of battery capacity fading mechanism in the lifecycle cost of electric bus fleet. IEEE Trans. Intell. Transport. Syst. 22 (4), 2371–2380. https://doi.org/10.1109/TITS.2020.3014097.

Zhou, Y., Meng, Q., Ong, G.P., 2022. Electric bus charging scheduling for a single public transport route considering nonlinear charging profile and battery degradation effect. Transp. Res. Part B Methodol. 159, 49–75. https://doi.org/10.1016/j.trb.2022.03.002.

Zhu, X., Yan, R., Huang, Z., Wei, W., Yang, J., Kudratova, S., 2020. Logistic optimization for multi depots loading capacitated electric vehicle routing problem from low carbon perspective. IEEE Access 8, 31934–31947. https://doi.org/10.1109/ACCESS.2020.2971220.